applied sciences

MDPI

Article

Simulation of Cross-Correlated Random Fields for Transversely Anisotropic Soil Slope by Copulas

Xinlong Zhou [1,2], Yueyang Sun [1,2] and Henglin Xiao [1,2,*]

[1] Technology Research Center of Ecological Road Engineering, Hubei University of Technology, Wuhan 430068, China; xlzhou@hbut.edu.cn (X.Z.); imrmei@hotmail.com (Y.S.)
[2] School of Civil Engineering, Architecture and Environment, Hubei University of Technology, Wuhan 430068, China
* Correspondence: xiaohenglin@hbut.edu.cn

Abstract: Multi-source uncertainties yielded by randomness, spatial variability and cross-correlation of soil parameters severely affect the realization of random fields. However, current studies rarely account for these simultaneously, leading to inevitable bias in random field simulation and subsequent structure analysis. In this paper, copula-based cross-correlated random fields for transversely anisotropic soil slope are proposed. Firstly, based on the traditional probabilistic method and random field theory, the effect of the cross-correlation of soil parameters on the random field is comprehensively analyzed. Then copulas, which mainly characterize the dependent structures of random variables, are further expanded to connect multivariate random fields. Four special algorithms associated with Gaussian, Frank, Plackett and No. 16 copulas are subsequently developed. At last, the performance and effectiveness of copula-based cross-correlated random fields are illustrated by means of assumed and engineering slope cases. The results show that the proposed method is amenable to characterizing spatial variability comprising multiple cross-correlated soil parameters of transversely anisotropic slope. Soil profiles can be represented with a relatively high accuracy. Moreover, the performance of copula-based CCRF is simultaneously governed by margins, cross-correlated coefficients and copulas. The proper selection of these crucial factors can considerably reduce multi-source uncertainties. Overall, the proposed method could provide a useful guideline for accurately modeling cross-correlation random fields of soil slope.

Keywords: spatial variability; cross-correlated random fields; transverse anisotropy; copula

Citation: Zhou, X.; Sun, Y.; Xiao, H. Simulation of Cross-Correlated Random Fields for Transversely Anisotropic Soil Slope by Copulas. *Appl. Sci.* **2023**, *13*, 4234. https://doi.org/10.3390/app13074234

Academic Editors: Susana Lopez-Querol and Pedro Navas

Received: 4 March 2023
Revised: 22 March 2023
Accepted: 24 March 2023
Published: 27 March 2023

1. Introduction

Due to internal material composition, stress environment, sedimentary conditions, weathering degree and burial conditions, natural soil materials show obvious randomness and spatial variability [1–6]. It is widely acknowledged that these two features make the real distribution of soil parameters more complex and trigger inevitable uncertainties [4,7–10]. Ignoring such uncertainties would lead to considerable deviation in geotechnical structure analyses, such as slope reliability. Therefore, it is essential that the accurate simulation of soil parameters with consideration of multisource uncertainties be conducted.

At present, the random variable model (RVM) and random field model (RFM) are commonly utilized to simulate spatially variable geotechnical parameters [11–14]. RVM assumes that each soil parameter in the same layer is homogeneous [11]. Its randomness and spatial variability are mainly characterized by random variables obeying specific probability distribution types, such as truncated normal (TN), lognormal (LN), truncated Gumbel (TG) and Weibull (WB) distributions [9,15]. However, soil parameters at any space location are supposed to be mutually independent of each other. This obviously does not reflect the real soil state. RFM is known to play an important role in modeling the spatial variability of soil parameters, and was first proposed by Vanmarcke in 1977 [13]. Compared

to RVM, it can account for the spatial correlation in the study area and can better describe spatial variability. Presently, great effort has been made in the generation of random fields of soil parameters [16–23]. For instance, Napoli et al. [19] studied rock slope stability by combining RFM with limit equilibrium methods. Pandit et al. [20] used the Fourier series method to generate an anisotropic random field. Yang et al. [21] combined the K-L series expansion method, the polynomial chaos expansion method and the Markov Chain Monte Carlo method to simulate spatially variable slopes. Liu et al. [22] simulated the spatially variable soil and carried out slope reliability analysis by the three-dimensional stochastic finite element method. Jiang et al. [23] established an effective non-stationary random field model for undrained shear strength parameters.

It is worth noting that the correlation of soil parameters is a crucial characteristic of the random field, including autocorrelation and cross-correlation [24]. The former characterizes the correlation of individual soil parameters at different spatial locations, mainly determined by the autocorrelation structure of soil parameter. The latter maintains that soil parameters also tend to be dependent on each other at a given spatial location or in neighborhoods. Both of them act as crucial constraints when simulating random fields. Many studies have claimed that interdependency among soil parameters could affect the distribution of random fields [4,24]. The challenge then for the geotechnical engineer is to model the spatially variable behavior of soil parameters that exhibit complex correlations. Unfortunately, cross-correlation is seldom considered in the simulation of random fields, which inevitably leads to huge bias in the generation of random fields. Such bias may further develop and expand in subsequent geotechnical structure analysis. These challenges highlight the significance of characterizing the spatial variability of soil profiles accounting for both autocorrelation and cross-correlation. Thus, a need to quantify both spatial variability and cross-correlation of soil parameters has arisen.

Fortunately, similar but limited efforts have been undertaken by some scholars [7,25,26]. Fenton and Griffiths [7] decomposed correlation matrices of parameters by Cholesky decomposition, and then simulated the cross-correlated random field (CCRF) using lower triangular matrices. Cho [25] assumed that all random fields have similar autocorrelation, and then used the cross-correlation coefficient to characterize the CCRFs of c and ϕ. However, according to probability theory, correlation coefficient cannot accurately represent the correlation structure among random variables. Such treatment obviously does not cater to the real spatial distribution of soil parameters. More efforts must be made to describe the correlation problem involving multiple-parameter random fields.

Copula theory has been gradually introduced to bridge the gap between individual margin and joint distribution [27–29]. It is capable of measuring complex interdependencies among random variables. To date, various related achievements have been made [9,14,15]. Presently, few studies have made attempts to expand copulas to characterize the relationship among multiple random fields [24,30,31]. Zhu et al. [24] proposed a framework of multivariate CCRF for geotechnical parameters. Subsequently, Wang and Li [30] discussed the application of copula theory in random field simulation. On the basis of these, Masoudian et al. [31] established a framework of multivariable CCRF under rainfall conditions by using copulas. However, similar studies on copula-based CCRF remain sparse. The performance and effectiveness of CCRF deserve to be further studied. On the other hand, previous studies mainly focused on Gaussian CCRFs. The effects of the non-Gaussian-dependent structure of soil parameters on anisotropic CCRF have seldom been reported. Therefore, more thorough efforts need to be taken to explore this controversial area.

To compensate for the aforementioned drawbacks, this paper is mainly intended to propose a new CCRF simulation method based on copulas. The remainder of the paper is organized as follows: brief introductions of random field theory and the copula theorem are elaborated in Sections 2 and 3, respectively; Section 4 establishes four algorithms associated with different candidate copulas; the overall simulation procedure of transversely anisotropic CCRF is displayed in Section 5; then the performance of the proposed method

is verified by means of an assumed soil slope and two engineering slope cases in Section 6; lastly, some outstanding conclusions are drawn in Section 7.

2. Random Field Theory

2.1. Overview

A random field, $\boldsymbol{H}(\mathbf{z}, \omega)$, is defined as a random function of variables $\mathbf{z} \in \Omega$, where Ω is the geometry of the spatial domain, and ω is a coordinate in the sample space [30,32]. At a given spatial coordinate, $\boldsymbol{H}(z_0, \omega)$ is a random variable that defines the spread in $\boldsymbol{H}$ at x_0. For a given outcome, $H(x, \theta_0)$ defines a realization of the field, which is a deterministic function in x. A specific random field $\boldsymbol{H}(\mathbf{z}, \omega)$ is usually based on its marginal distribution $H(\mathbf{z}, \omega) \sim f(\mu(\mathrm{z}), \sigma(\mathrm{z}))$ and autocorrelation function (ACF) $\rho(\mathrm{z}, \mathrm{z}') = \rho(\|\mathrm{z}\text{-}\mathrm{z}'\|, \delta)$, where $\mu(\mathrm{z}) = E[\boldsymbol{H}(\mathbf{z}, \omega)]$ and $\sigma^2(\mathrm{z}) = E[(\boldsymbol{H}(\mathbf{z}, \omega) - \mu(\mathrm{z}))^2]$ are the mean and variance, respectively; $\|\mathrm{z}\text{-}\mathrm{z}'\|$ is the relative distance between any two points in the field, and δ is the scale of fluctuation (SOF). Different types of anisotropic random fields have different autocorrelation functions. As for two-dimensional random fields, the SOFs can be divided into horizontal and vertical, defined as δ_h and δ_v, respectively. According to previous studies [33,34], δ_h belongs to 10–80 m and δ_v is 0.2–6 m. The mean value $\mu(z)$, variance σ^2 and CDF $F(z)$ can be obtained from the in-situ data. When $\mu(z)$ and σ^2 are assumed to be unchanged with soil depth, this is called a stationary random field.

2.2. Transversely Anisotropic Random Field

A stationary random field can be divided into two types: isotropic random field and anisotropic random field [35]. In the former, the material properties and SOF are independent of the direction. In contrast, the latter is characterized by the direction-dependency of SOF, which is represented by the main SOF δ_1, the secondary SOF δ_2 and the direction angle φ. The spatial variation of random variables is the smoothest along the direction of δ_1, and the roughest in the direction of δ_2. A transversely anisotropic random field is a special case of the anisotropic random field. Soil parameters change smoothly in the direction of δ_1, and faster in the direction of δ_2.

To characterize isotropic and transversely anisotropic random fields, SOF and ACF must be formulated. As for ACF, theoretical ACFs are generally employed to approximate the autocorrelation. Notably, exponential ACF is the most commonly used in geotechnical engineering. In this paper, soil parameters are also assumed to obey an exponential autocorrelation structure.

The formulation of SOF in the isotropic case is circular and direction-independent, namely, $\delta_1 = \delta_2$. Then, the theoretical formulation of SOF δ_φ at directional angle φ can be expressed as below [35]:

$$\delta_\varphi = \delta_1 = \delta_2 \tag{1}$$

The corresponding exponential ACF is:

$$\rho = \exp\left[-2\frac{\sqrt{\Delta x^2 + \Delta y^2}}{\delta_\varphi}\right] \tag{2}$$

where Δx and Δy, respectively, represent absolute horizontal and vertical distances between two spatial locations.

As for anisotropic random fields, the formulation of SOF is generally assumed as an ellipse and is parameterized by using δ_φ, δ_1 and δ_2.

$$\frac{(\delta_\varphi \cos\varphi)^2}{\delta_1^2} + \frac{(\delta_\varphi \sin\varphi)^2}{\delta_2^2} = 1 \tag{3}$$

Via trigonometric transformation, Equation (3) can be transformed as

$$\frac{\delta_\varphi^2 \frac{1}{1+\tan^2\varphi}}{\delta_1^2} + \frac{\delta_\varphi^2 \frac{\tan^2\varphi}{1+\tan^2\varphi}}{\delta_2^2} = 1 \tag{4}$$

Let

$$\tan\varphi = \frac{\Delta y}{\Delta x} \tag{5}$$

Substituting Equation (5) into Equation (4) yields

$$\sqrt{\left(\frac{\Delta x}{\delta_1}\right)^2 + \left(\frac{\Delta y}{\delta_2}\right)^2} = \frac{\sqrt{\Delta x^2 + \Delta y^2}}{\delta_\varphi} \tag{6}$$

According to the definition of a transversely anisotropic random field, the spatial variation of random variables is the smoothest in the direction of δ_1, and the roughest in the direction of δ_2. Assuming that the formulation of SOF is elliptical, δ_φ can be expressed as

$$\delta_\varphi = \sqrt{\frac{\delta_1^2\delta_2^2(1+\tan^2\varphi)}{\delta_2^2 + \delta_1^2\tan^2\varphi}} \tag{7}$$

The corresponding exponential ACF is:

$$\rho = \exp\left[-2\sqrt{\frac{\Delta x^2}{\delta_1^2} + \frac{\Delta y^2}{\delta_2^2}}\right] \tag{8}$$

2.3. Discretization of Transversely Anisotropic Random Field

The discretization method is crucial to the construction of a random field. At present, several approaches have been provided to approach this, such as the local average method, covariance matrix decomposition method, Fourier transform method and Karhunen–Loève series expansion method. Due to its capability of dealing with space transformation problems, covariance matrix decomposition is adopted to discretize random fields.

The autocorrelation matrix $\mathbf{M}_a$ can be established by discretizing the random field at the centroid of random field elements [24]:

$$\mathbf{M}_a = \begin{bmatrix} 1 & \rho(\Delta x_{12}, \Delta y_{12}) & \cdots & \rho(\Delta x_{1n_e}, \Delta y_{1n_e}) \\ \rho(\Delta x_{21}, \Delta y_{21}) & 1 & \cdots & \rho(\Delta x_{2n_e}, \Delta y_{2n_e}) \\ \vdots & \vdots & \ddots & \vdots \\ \rho(\Delta x_{n_e1}, \Delta y_{n_e1}) & \rho(\Delta x_{n_e2}, \Delta y_{n_e2}) & \cdots & 1 \end{bmatrix} \tag{9}$$

wherein ρ represents the autocorrelation coefficient between any two locations; Δx_{ij} and Δy_{ij} represent the absolute horizontal and vertical distances between the centroids of the i-th and the j-th elements; n_e is the number of elements.

Via the Cholesky decomposition method, $\mathbf{M}_a$ can be decomposed into the product of lower triangular matrix $\mathbf{L}$ and its transpose:

$$\mathbf{L} \cdot \mathbf{L}^T = \mathbf{M}_a \tag{10}$$

Via $\mathbf{L}$, the standard normal random field $\boldsymbol{H}^G$ can be obtained:

$$\mathbf{H}^G = \mathbf{L} \cdot \mathbf{Z} \tag{11}$$

wherein $\mathbf{Z}$ is the independent standard normal random variables. With the aid of the mean, standard deviation and margins of random variables, $\boldsymbol{H}^G$ can be transformed into the expected non-normal random field.

In this paper, the transversely isotropic random field with an exponential correlation structure is studied. Substituting Equation (8) into Equation (9) yields the autocorrelation matrix of transversely anisotropic random fields. According to Equations (10) and (11), an independent standard Gaussian random field $\boldsymbol{H}^{IAG}$ can be obtained by setting $\mu = 0$ and $\sigma = 1$. Figure 1 shows a standard normal random field in a 100 × 100 grid, where $\delta_1 = 20$ and $\delta_2 = 2$, respectively. Given the mean, standard deviation and probability distribution, the independent transversely isotropic standard normal random field $\boldsymbol{H}^{IAG}$ in Figure 1 can be transformed into the desired non-Gaussian field.

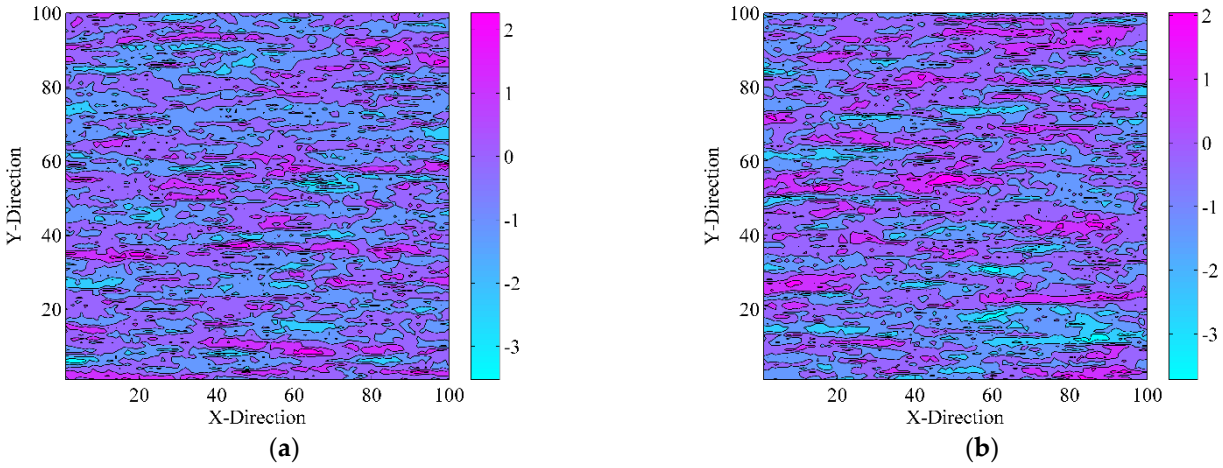

Figure 1. Independent standard normal and transversely anisotropic random field $\boldsymbol{H}^{IAG}$. (**a**) Random field of u. (**b**) Random field of v.

3. Copula Theory

$F_1(X_1)$, $F_2(X_2)$, ..., and $F_m(X_m)$ are marginal distributions of random variables $\boldsymbol{X} = (X_1, X_2, \cdots, \text{and } X_m)$. Via Sklar's theory, the joint CDF $F_{\boldsymbol{X}}(X_1, X_2, \cdots, X_m)$ can be expressed by an unique copula function $\boldsymbol{C}$ [27]:

$$F_X(\boldsymbol{X}) = \boldsymbol{C}[(F_1(X_1), F_2(X_2), \cdots, F_m(X_m); \boldsymbol{\theta}] \tag{12}$$

wherein $\boldsymbol{C}$ is uncorrelated with each margin; $\boldsymbol{\theta}$ represents the copula parameter.

Specifically, while $\boldsymbol{X}$ is mutually independent, Equation (12) can be rewritten as

$$F_X(\boldsymbol{X}) = \prod_{j=1}^{m} F_j(X_j) \tag{13}$$

By differentiating Equation (12), the joint PDF $f_{\boldsymbol{X}}(X_1, X_2, \cdots, \text{and } X_m)$ can be derived:

$$f_X(\boldsymbol{X}) = \boldsymbol{D}[F_1(X_1), F_2(X_2), \cdots, F_m(X_m); \boldsymbol{\theta}] \prod_{j=1}^{m} f_j(X_j) \tag{14}$$

where in $f_1(x_1), f_2(x_2), \ldots$, and $f_m(x_m)$ are marginal PDFs of $\boldsymbol{X}$ and $\boldsymbol{D}(\cdot)$ is the copula PDF; when variables are mutually independent, $\boldsymbol{D}(\cdot) = 1$.

Table 1 gives some candidate copulas commonly used in soil slope analysis. It is noted that the copula parameter $\boldsymbol{\theta}$ is crucial to constructing the copula. Commonly, maximum likelihood estimation is used to estimate $\boldsymbol{\theta}$, as expressed below [27].

$$L(\boldsymbol{\theta}) = \prod_{i=1}^{n} \boldsymbol{D}(u_1, u_2, \cdots u_m; \boldsymbol{\theta}) = \prod_{j=1}^{m} \frac{\partial^m \boldsymbol{C}(u_1, u_2, \cdots, u_m; \boldsymbol{\theta})}{\partial u_1 \partial u_2 \cdots \partial u_m} \tag{15}$$

wherein u_1, u_2, ... , and u_m can be represented by transforming $\boldsymbol{X}$ from original space into rank space, as shown below.

$$u_j^{(i)} = \frac{rank(X_j^{(i)})}{n+1}, i = 1, 2, \cdots, n \tag{16}$$

Table 1. CDFs and PDFs of candidate copulas.

Copula	$C(u,v;\theta)$	$c(u,v;\theta)$	θ
Gaussian	$\Phi_\theta\left(\Phi^{-1}(u), \Phi^{-1}(v)\right)$	$\Phi\left(\frac{\Phi^{-1}(u_2)-\theta\Phi^{-1}(u_1)}{\sqrt{1-\theta^2}}\right)$	[–1, 1]
Plackett	$\frac{S-\sqrt{S^2-4uv\theta(\theta-1)}}{2(\theta-1)}$, $S = 1+(\theta-1)(u+v)$	$\frac{1}{2} - \frac{1+(\theta-1)u_1-(\theta+1)u_2}{2\left\{[1+(\theta-1)(u_1+u_2)]^2-4u_1u_2\theta(\theta-1)\right\}^{\frac{1}{2}}}$	$(0, +\infty)\backslash\{1\}$
Frank	$-\frac{1}{\theta}\ln\left[1+\frac{(e^{-\theta u}-1)(e^{-\theta v}-1)}{e^{-\theta}-1}\right]$	$\frac{e^{-\theta u_1}(e^{-\theta u_2}-1)}{(e^{-\theta}-1)+(e^{-\theta u_1}-1)(e^{-\theta u_2}-1)}$	$(-\infty, +\infty)\backslash\{0\}$
No. 16	$\frac{1}{2}\left(S+\sqrt{S^2+4\theta}\right)$, $S = u_1+u_2-1-\theta\left(\frac{1}{u_1}+\frac{1}{u_2}-1\right)$	$\frac{1}{2}\left(1+\frac{\theta}{u_1^2}\right)\left[1+S(S^2+4\theta)^{-\frac{1}{2}}\right]$, $S = u_1+u_2-1-\theta\left(\frac{1}{u_1}+\frac{1}{u_2}-1\right)$	$[0, +\infty)$

For simplification, the logarithm form of $\ln L(\boldsymbol{\theta})$ is computed based on the following equation

$$\ln L(\boldsymbol{\theta}) = \prod_{j=1}^{m} \boldsymbol{D}(u_1, u_2, \cdots u_m; \boldsymbol{\theta}) = \sum_{j=1}^{m} \ln \boldsymbol{D}(u_1, u_2, \cdots u_m) \tag{17}$$

Via solving Equation (17), the maximum likelihood estimator $\hat{\boldsymbol{\theta}}_{ML}$ that satisfies $\ln L(\hat{\boldsymbol{\theta}}_{ML}) \geq \ln L(\boldsymbol{\theta})$ can be obtained.

$$\frac{\partial \ln L(\boldsymbol{\theta})}{\partial \boldsymbol{\theta}} = 0 \tag{18}$$

From Equations (12) and (14), it can be found that different copulas describe different dependent structures. Therefore, the optimal copula should be sieved out first. Generally, the Akaike Information Criterion (AIC) [36] and Bayesian Information Criterion (BIC) [37] are adopted to sieve out the proper candidate copula, as briefly expressed below,

$$AIC = 2k - 2\sum_{j=1}^{m} \ln \boldsymbol{D}(u_1, u_2, \cdots, u_m) \tag{19}$$

$$BIC = k \cdot \ln n - 2\sum_{j=1}^{m} \ln \boldsymbol{D}(u_1, u_2, \cdots, u_m) \tag{20}$$

where k is the number of parameters concerning the estimated model. The model associated with minimum AIC and BIC scores is considered the preferable candidate.

4. Simulation of CCRF from Copula Aspect

4.1. Cross-Correlation of Soil Parameters

As aforementioned, soil parameters show two types of correlations, namely, autocorrelation and cross-correlation, as demonstrated in Figure 2. The former characterizes the correlation of individual soil parameters at different spatial locations, mainly determined by the autocorrelation structure of the parameter. In this paper, exponential ACF is used to replace it. The latter maintains that soil parameters also tend to be dependent on each other at a given spatial location or neighborhoods, commonly measured by their cross-correlation coefficients. For example, c and ϕ, which are key parameters affecting slope stability, have been proven to be negatively correlated. This implies that c and ϕ

should appear dependently in any spatial location. Therefore, to consider the spatial variability and cross-correlation simultaneously, all these parameters should be simulated as cross-correlation random fields, as shown in Figure 2.

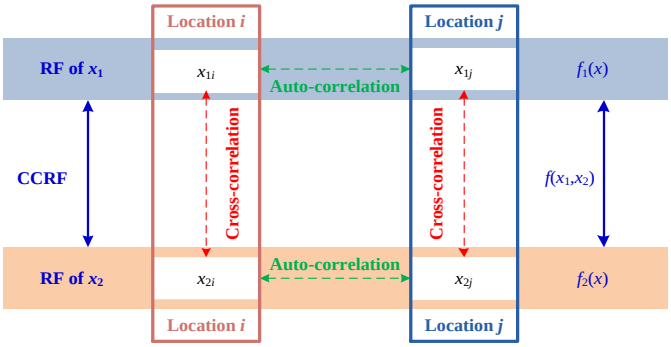

Figure 2. Schematic diagram of correlations among soil parameters.

Some scholars have studied such cross-correlation and claimed that the heterogeneity and cross-correlation of soil profiles severely affect the stability of geotechnical structures. Fenton and Griffiths [7] decomposed correlation matrices of parameters using the Cholesky decomposition method, and then simulated the CCRF using lower triangular matrices. Cho [25] assumes that all random fields simulated in the same space have the same ACF. Then, the cross-correlation coefficient was used to characterize the cross-correlation between random fields of c and ϕ. The influence of cross-correlation on slope reliability was properly accounted for. However, according to copula theory, the correlation coefficient cannot accurately capture the correlation structure among parameters. To solve this problem, copula theory can be introduced to quantify the cross-correlation of soil parameters. Copulas are able to measure complex interdependencies among soil parameters. This might be expanded to make up for the deficiency of the traditional cross-correlation coefficient in simulating CCRF. To this end, copulas are intended to link individual random fields, as illustrated in the next section.

4.2. Transformation of CCRF by Copulas

As discussed in the previous section, a dependence structure exists among soil parameters. Random fields corresponding to different soil parameters are therefore correlated with each other. However, the cross-correlation coefficient matrix cannot accurately represent the cross-correlation between random fields. The key issue to be solved in this section is how to connect the independent standard normal random fields $\boldsymbol{H}^{IAG}$ with a specific correlation structure or a copula function. In essence, simulating CCRF is still a construction process of the joint distribution of multiple random variables, which obey the specified dependence structure. Therefore, $\boldsymbol{H}^{IAG}$ can be first converted into an independent standard uniform random field $\boldsymbol{H}^{CAU}$. Then, multivariate CCRFs can be constructed according to the predefined copula.

The general framework for generating a cross-correlation standard uniform random field $\boldsymbol{H}^{CAU}$ based on copula function is as follows.

The proposed copula-based CCRF is advantageous in that it can efficiently capture the interdependency of soil parameters. If required, $(\boldsymbol{H}_1{}^{CAU}, \boldsymbol{H}_2{}^{CAU}, \cdots, \boldsymbol{H}_i{}^{CAU})$ can readily be converted into expected non-Gaussian random fields by giving the mean, standard deviation and marginal probability distribution of soil parameters.

It is worth noting that dependent structures characterized by different copulas are severely different. This implies that the CCRFs simulated by different copulas also differ from each other. Care must be taken to ensure the selected copula matches the target interdependency of soil parameters. Such matching is commonly achieved through goodness-of-fit tests. Namely, Algorithm 1 should be modified to cater to real spatial correlation based on specific copulas. Fortunately, several efforts have been made by us and other researchers.

Gaussian, Plackett, Frank and No. 16 copulas, as shown in Table 1, have been proven to be able to match the requirements. To this end, the four candidates are also employed to exploit transversely anisotropic CCRF in the subsequent sections.

Algorithm 1 Simulation algorithm of copula-based standard uniform CCRF

(1) Define the correlation structure between multivariate correlation standard uniform random fields as $C_i = C$ ($\boldsymbol{H}_1{}^{CAU}$, $\boldsymbol{H}_2{}^{CAU}$, $\cdots$, $\boldsymbol{H}_i{}^{CAU}$), where $i = 2, 3, \cdots, n$;
(2) Extract $\boldsymbol{H}_1{}^{IAU}$ from the standard uniform distribution U(0, 1), let $\boldsymbol{H}_1{}^{CAU} = \boldsymbol{H}_1{}^{IAU}$;
(3) Extract $\boldsymbol{H}_2{}^{CAU}$ from C_2 ($\boldsymbol{H}_2{}^{CAU} \mid \boldsymbol{H}_1{}^{CAU}$);
(4) Similarly, extract $\boldsymbol{H}_n{}^{CAU}$ from C_n ($\boldsymbol{H}_n{}^{CAU} \mid \boldsymbol{H}_1{}^{CAU}$, $\boldsymbol{H}_2{}^{CAU}$, $\cdots$, $\boldsymbol{H}_{n-1}{}^{CAU}$).

4.3. Gaussian Copula-Based CCRF

In the previous section, a framework of copula-based standard uniform CCRF has been established. As soil parameters obeying Gaussian copula, the simulation approach of Gaussian Copula-based CCRF is displayed in Algorithm 2.

Algorithm 2 Simulation algorithm of Gaussian copula-based CCRF

(1) Define the independent standard normal random fields of x and y as $\boldsymbol{H}^{IAG} = [\, \boldsymbol{H}_x{}^{IAG}, \boldsymbol{H}_y{}^{IAG} \,]^{\mathrm{T}}$.
(2) Perform Cholesky decomposition on the correlation coefficient matrix $\boldsymbol{\theta}$ composed of Gaussian copula parameter θ to obtain the lower triangular matrix $\boldsymbol{L}_0$.
(3) Let $\boldsymbol{H}^{CAG} = \boldsymbol{L}_0\boldsymbol{H}^{IAG}$, then the cross-correlation standard normal random fields $\boldsymbol{H}^{CAG} = [\boldsymbol{H}_x{}^{CAG}, \boldsymbol{H}_y{}^{CAG}\,]^{\mathrm{T}}$ can be obtained.
(4) Let $\boldsymbol{H}^{CAU} = \Phi(\boldsymbol{H}^{CAG})$, where $\Phi(\cdot)$ is the CDF of the standard normal distribution, and the cross-correlation standard uniform random fields of x and y can be obtained $\boldsymbol{H}^{CAU} = [\boldsymbol{H}_x{}^{CAU}, \boldsymbol{H}_y{}^{CAU}\,]^{\mathrm{T}}$.
(5) Define ${F_x}^{-1}(\cdot)$ and ${F_y}^{-1}(\cdot)$ as the inverse functions of the CDF of x and y, respectively. Perform isoprobabilistic transformation on $\boldsymbol{H}^{CAU}$ to obtain the cross-correlation non-normal random fields of x and y $\boldsymbol{H}^{CAN} = [\boldsymbol{H}_x{}^{CAN}, \boldsymbol{H}_y{}^{CAN}\,]^{\mathrm{T}} = [{F_x}^{-1}(\boldsymbol{H}_x{}^{CAU}), {F_y}^{-1}(\boldsymbol{H}_y{}^{CAU})]^{\mathrm{T}}$.

4.4. Plackett Copula-Based CCRF

As soil parameters obeying the Plackett copula, the simulation approach of the Plackett copula-based CCRF is shown in Algorithm 3.

Algorithm 3 Simulation algorithm of Plackett copula-based CCRF

(1) Define the independent standard normal random fields x and y $\boldsymbol{H}^{IAG} = [\boldsymbol{H}_x{}^{IAG}, \boldsymbol{H}_y{}^{IAG}\,]^{\mathrm{T}}$.
(2) Let $\boldsymbol{H}^{IAU} = \Phi(\boldsymbol{H}^{IAG})$, then the independent standard uniform random fields of x and y $\boldsymbol{H}^{IAU} = [\boldsymbol{H}_x{}^{IAU}, \boldsymbol{H}_y{}^{IAU}]^{\mathrm{T}}$ can be obtained.
(3) Define $\boldsymbol{a} = \boldsymbol{H}_y{}^{IAU}\,(1-\boldsymbol{H}_y{}^{IAU})$, $\boldsymbol{b} = \theta + \boldsymbol{a}(\theta-1)^2$, $\boldsymbol{c} = 2\boldsymbol{a}\,(\boldsymbol{H}_x{}^{IAU}\theta^2 + 1\text{-}\boldsymbol{H}_x{}^{IAU}) + \theta\,(1\text{–}2\boldsymbol{a}_0)$, $\boldsymbol{d} = \theta^{1/2}[\,\theta + 4\boldsymbol{a}\boldsymbol{H}_x{}^{IAU}(1-\boldsymbol{H}_x{}^{IAU})(1-\theta)^2\,]^{1/2}$.
(4) Let $\boldsymbol{H}_x{}^{CAU} = \boldsymbol{H}_x{}^{IAU}$, $\boldsymbol{H}_y{}^{CAU} = [\boldsymbol{c}\text{-}(1\text{–}2\boldsymbol{H}_y{}^{IAU})\boldsymbol{d}\,]/2\boldsymbol{b}$, and obtain the cross-correlation standard uniform random fields x and y $\boldsymbol{H}^{CAU} = [\,\boldsymbol{H}_x{}^{CAU}, \boldsymbol{H}_y{}^{CAU}]^{\mathrm{T}}$.
(5) Use ${F_x}^{-1}(\cdot)$ and ${F_y}^{-1}(\cdot)$ to perform isoprobabilistic transformation on $\boldsymbol{H}^{CAU} = [\boldsymbol{H}_x{}^{CAU}, \boldsymbol{H}_y{}^{CAU}]$. Then the cross-correlation non-normal random fields of x and y $\boldsymbol{H}^{CAN} = [\boldsymbol{H}_x{}^{CAN}, \boldsymbol{H}_y{}^{CAN}\,]^{\mathrm{T}} = [{F_x}^{-1}(\boldsymbol{H}_x{}^{CAU}), {F_y}^{-1}(\boldsymbol{H}_y{}^{CAU})]^{\mathrm{T}}$ can be obtained.

4.5. Frank Copula-Based CCRF

As soil parameters obeying the Frank copula, the simulation of the Frank copula-based CCRF can be implemented by Algorithm 4.

Algorithm 4 Simulation algorithm of Frank copula-based CCRF

(1) Define the independent standard normal random fields of x and y $\boldsymbol{H}^{IAG} = [\boldsymbol{H}_x{}^{IAG}, \boldsymbol{H}_y{}^{IAG}]^{\mathrm{T}}$.
(2) Let $\boldsymbol{H}^{IAU} = \Phi(\boldsymbol{H}^{IAG})$, then the independent standard uniform random fields of x and y $\boldsymbol{H}^{IAU} = [\boldsymbol{H}_x{}^{IAU}, \boldsymbol{H}_y{}^{IAU}]^{\mathrm{T}}$ can be obtained.
(3) Let $\boldsymbol{H}_x{}^{CAU} = \boldsymbol{H}_x{}^{IAU}$, $\boldsymbol{H}_y{}^{CAU}$ be inversely calculated according to the Frank copula, as shown below:

$$\boldsymbol{H}_y^{CAU} = -\frac{1}{\theta}\ln\left[\frac{1+\boldsymbol{H}_y^{IAU}(e^{-\theta}-1)}{e^{-\theta\boldsymbol{H}_x^{IAU}}-\boldsymbol{H}_y^{IAU}(e^{-\theta\boldsymbol{H}_x^{IAU}}-1)}\right]$$

(4) Solve the above equation in (3) to get the cross-correlation standard uniform random fields $\boldsymbol{H}^{CAU} = [\boldsymbol{H}_x{}^{CAU}, \boldsymbol{H}_y{}^{CAU}]^{\mathrm{T}}$ of x and y.
(5) Use $F_x{}^{-1}(\cdot)$ and $F_y{}^{-1}(\cdot)$ to perform isoprobabilistic transformation on $\boldsymbol{H}^{CAU} = [\boldsymbol{H}_x{}^{CAU}, \boldsymbol{H}_y{}^{CAU}]$. Then the cross-correlation non-normal random fields of x and y $\boldsymbol{H}^{CAN} = [\boldsymbol{H}_x{}^{CAN}, \boldsymbol{H}_y{}^{CAN}]^{\mathrm{T}} = [F_x{}^{-1}(\boldsymbol{H}_x{}^{CAU}), F_y{}^{-1}(\boldsymbol{H}_y{}^{CAU})]^{\mathrm{T}}$ can be obtained.

4.6. No. 16 Copula-Based CCRF

As soil parameters obeying No. 16 copula, the simulation of No. 16 copula-based CCRF can be carried out by Algorithm 5.

Algorithm 5 Simulation algorithm of No. 16 copula-based CCRF

(1) Define the independent standard normal random fields of x and y as $\boldsymbol{H}^{IAG} = [\boldsymbol{H}_x{}^{IAG}, \boldsymbol{H}_y{}^{IAG}]^{\mathrm{T}}$.
(2) Let $\boldsymbol{H}^{IAU} = \Phi(\boldsymbol{H}^{IAG})$, then the independent standard uniform random fields of x and y $\boldsymbol{H}^{IAU} = [\boldsymbol{H}_x{}^{IAU}, \boldsymbol{H}_y{}^{IAU}]^{\mathrm{T}}$ can be obtained.
(3) Let $\boldsymbol{H}_x{}^{CAU} = \boldsymbol{H}_x{}^{IAU}$, $\boldsymbol{H}_y{}^{CAU}$ be calculated according to the following equation:

$$\begin{cases} \boldsymbol{H}_y^{IAU} = \frac{1}{2}(1+\theta/(\boldsymbol{H}_x^{IAU})^2)\left[1+S(S^2+4\theta)-1/2\right] \\ S = \boldsymbol{H}_x^{IAU}+\boldsymbol{H}_y^{CAU}-1-\theta(1/\boldsymbol{H}_x^{IAU}+1/\boldsymbol{H}_y^{CAU}-1) \end{cases}$$

(4) Solve equations in (3) to get the cross-correlation standard uniform random fields $\boldsymbol{H}^{CAU} = [\boldsymbol{H}_x{}^{CAU}, \boldsymbol{H}_y{}^{CAU}]^{\mathrm{T}}$ of x and y.
(5) Use $F_x{}^{-1}(\cdot)$ and $F_y{}^{-1}(\cdot)$ to perform isoprobabilistic transformation on $\boldsymbol{H}^{CAU} = [\boldsymbol{H}_x{}^{CAU}, \boldsymbol{H}_y{}^{CAU}]$. Then the cross-correlation non-normal random fields of x and y $\boldsymbol{H}^{CAN} = [\boldsymbol{H}_x{}^{CAN}, \boldsymbol{H}_y{}^{CAN}]^{\mathrm{T}} = [F_x{}^{-1}(\boldsymbol{H}_x{}^{CAU}), F_y{}^{-1}(\boldsymbol{H}_y{}^{CAU})]^{\mathrm{T}}$ can be obtained.

5. Simulation Process of Transversely Anisotropic CCRF

To model ideal CCRFs, the random field is firstly discretized by the matrix decomposition method with consideration of the spatial variability of soil parameters. Then, copulas are employed to model the cross-correlation of random fields. Thus, the multivariate CCRFs are constructed to accurately represent the spatially variable soil profiles. The simulation procedures of transversely anisotropic CCRF are as follows:

Step 1: Characterize the slope geometry and collect on-site data of mechanical parameters. Then the random variable $\boldsymbol{X}$ of the soil parameters and corresponding statistics can be determined;

Step 2: Determine the optimal marginal distribution $F(\cdot)$ and copula function $C(\cdot)$ of soil parameters. According to our previous studies, TN, LN, GB and WB are selected as candidate margins. Gaussian, Plackett, Frank and No. 16 copulas are chosen to be candidates. Via AIC and BIC, the optimal copulas and margins are sieved out;

Step 3: Establish a geometric model of the studied slope. Boundary conditions are set and finite element meshes are divided. Then the finite element analysis model is established. Slope stability analysis is carried out in the "job" module. Develop a MATLAB program to extract the meshes, node coordinates and other related information from the "*.inp" file automatically generated by ABAQUS;

Step 4: Substitute the node and element coordinates obtained in ***Step 3*** into Equation (9) to calculate the autocorrelation matrix $\mathbf{M}_a$. According to Equation (10), perform Cholesky decomposition and obtain the lower triangular matrix $\mathbf{L}$. Subsequently, independent standard normal random fields $\boldsymbol{H}^{IAG}$ are generated from Equation (11). It should be

pointed out that the mesh size of CCRF model used in this paper is consistent with that of the finite element model;

Step 5: According to the copula determined in ***Step 2***, the corresponding CCRF algorithm is selected. Then the cross-correlation standard uniform random fields $\boldsymbol{H}^{CAU}$ are established. Via the inverse function $F^{-1}(\cdot)$ of the margins of soil parameters determined in ***Step 2***, $\boldsymbol{H}^{CAU}$ is converted into the expected cross-correlation non-normal random fields $\boldsymbol{H}^{CAN}$ by isoprobabilistic transformation.

6. Numerical Illustrations

In this section, the performance of the proposed copula-based CCRF method is demonstrated by means of three numerical examples. The first considers a classical *c*-ϕ soil slope. The feasibility of the proposed method is validated. The effects of copulas, margins and the difference between the cross-correlation and dependent structure are deeply explored using this example. The second is the Chicago Congress Street cut slope with measured statistics of soil parameters. The slope has four soil layers with different features. The performance of the proposed method in modeling multi-layer CCRF is demonstrated. The last considers the Papillion River Basin slope in the United States. A set of on-site observations of soil parameters is available. The application of the proposed method is verified.

6.1. Example 1: Assumed c-ϕ Soil Slope

6.1.1. Profiles of *c*-ϕ Soil Slope

To illustrate the feasibility and effectiveness of the proposed copula-based CCRF, a widely used assumed *c*-ϕ soil slope is adopted [3]. Figure 3 shows the geometry of the studied slope, discretized by 1243 four-noded quadrilateral elements, wherein the lower boundary is fixed, and the left and right boundaries are fixed horizontally. For simplification, the influence of groundwater level is ignored here. Generally, soil parameters c and ϕ show considerable randomness, spatial variability and cross-correlation. They are therefore regarded as random variables, both of which are assumed to obey LN distribution. Corresponding statistics are shown in Table 2. Other slope profiles are shown in Table 3.

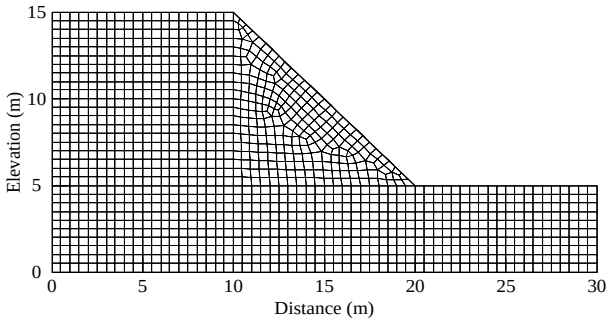

Figure 3. Assumed *c*-ϕ slope.

Table 2. Statistics and random field parameters of the assumed soil slope.

Parameters	μ	COV	Margin	SOF	Cross-Correlation
c	10 kPa	0.3	Lognormal	δ_h = 20 m, δ_v = 2 m	$\rho_{c,\phi} = -0.5$
ϕ	30°	0.2	Lognormal	δ_h = 20 m, δ_v = 2 m	

Table 3. The profiles of the assumed soil slope.

Parameter	Height	Slope Angle	Elastic Modulus	Poisson's Ratio	Unit Weight
Value	10 m	45°	35 MPa	0.35	20 kN/m^3

6.1.2. Simulation of CCRF

In this section, bivariate CCRFs of c and ϕ are established according to Algorithms 1–4. Then, their performances and differences are discussed in detail.

Figures 4–7 respectively display the typical realizations of CCRFs associated with four candidate copulas. In the subfigures of the slope geometry, the depth of mesh color represents the magnitude of soil parameters. Namely, the deeper the color, the larger the value of c or ϕ. It is evident that spatially variable soil properties can be efficiently demonstrated by the CCRF models. Soil parameters c and ϕ develop smoothly in the horizontal direction, but fluctuate severely in the vertical direction. This is mainly attributed to the domination of SOFs δ_h and δ_v. As δ_v is much smaller than δ_h (2 m vs. 20 m), c and ϕ fluctuate more severely in the vertical direction than in the horizontal direction, further indicating the reasonable characterization of spatial variability. In addition, it can also be clearly observed from Figures 4–7 that as c develops a deeper color, the corresponding ϕ in the same location develops a lighter color, and vice versa. This indicates that a negative cross-correlation exhibits between the two random fields.

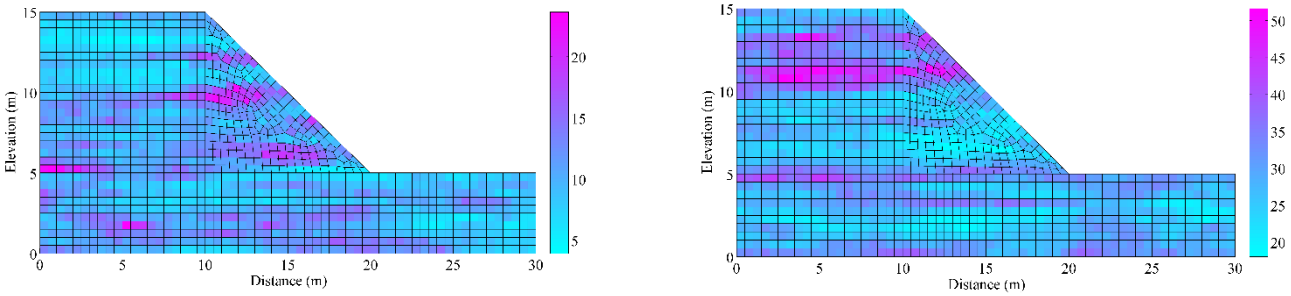

(**a**) (**b**)

Figure 4. A typical realization of Gaussian copula-based transversely anisotropic CCRF. (**a**) Random field of c. (**b**) Random field of ϕ.

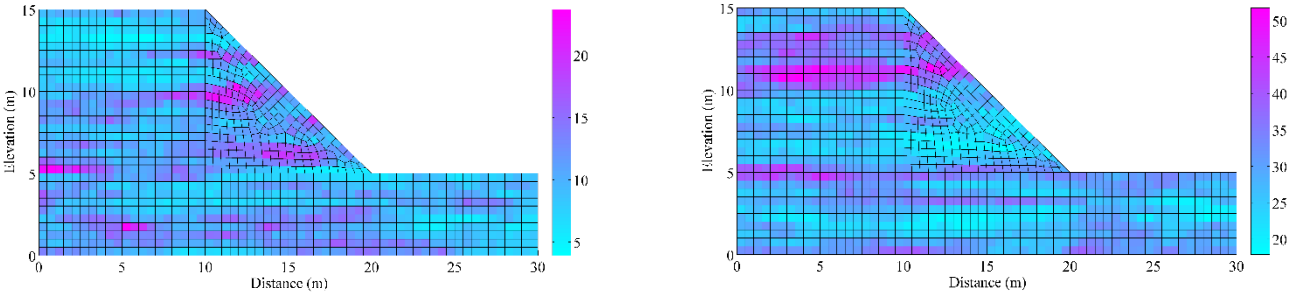

(**a**) (**b**)

Figure 5. A typical realization of Plackett copula-based transversely anisotropic CCRF. (**a**) Random field of c. (**b**) Random field of ϕ.

The above ratiocinations can be further validated using the corresponding scatter plots in Figure 8. As expected, all the four candidate copulas yield negative dependence structures, which are consistent with the presented correlation direction. The copulas seem to be sufficient to give an excellent description of the cross-correlation of soil parameters. However, the realizations of CCRF and scatter plots of soil parameters associated with different copulas are comparably inconsistent, especially for the No. 16 copula. Such discrepancies with respect to Gaussian, Plackett and Frank copulas are comparatively unobvious. These may further propagate and affect the final geotechnical structure analysis. To this end, it can be concluded that different copulas correspond to different CCRF models and interdependencies. The performance of copula-based CCRF is simultaneously governed by dependent structures and cross-correlations of random variables.

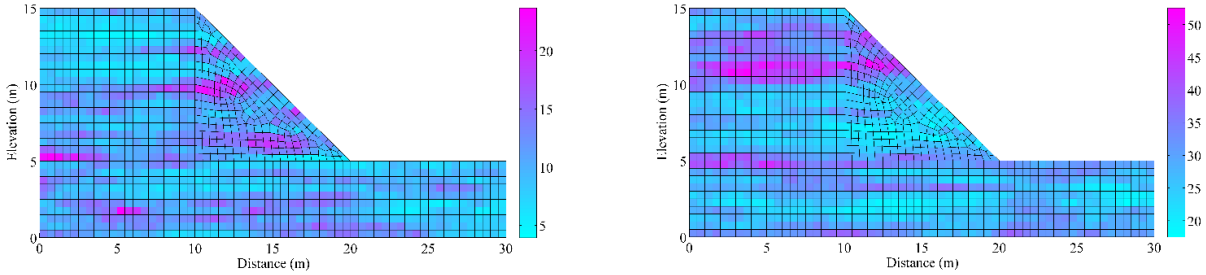

(**a**) (**b**)

Figure 6. A typical realization of Frank copula-based transversely anisotropic CCRF. (**a**) Random field of c. (**b**) Random field of ϕ.

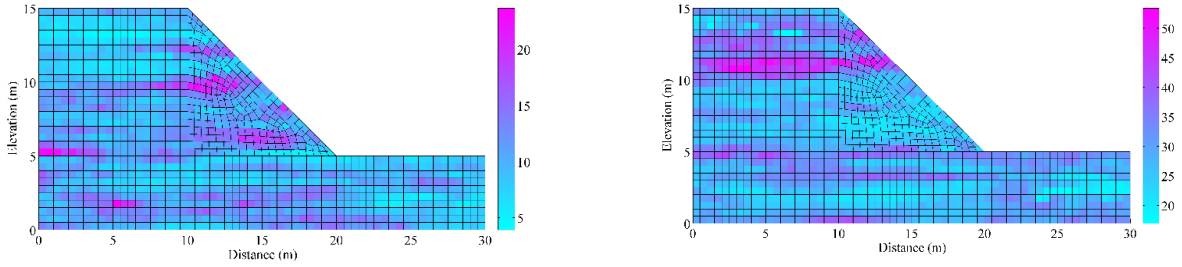

(**a**) (**b**)

Figure 7. A typical realization of No. 16 copula-based transversely anisotropic CCRF. (**a**) Random field of c. (**b**) Random field of ϕ.

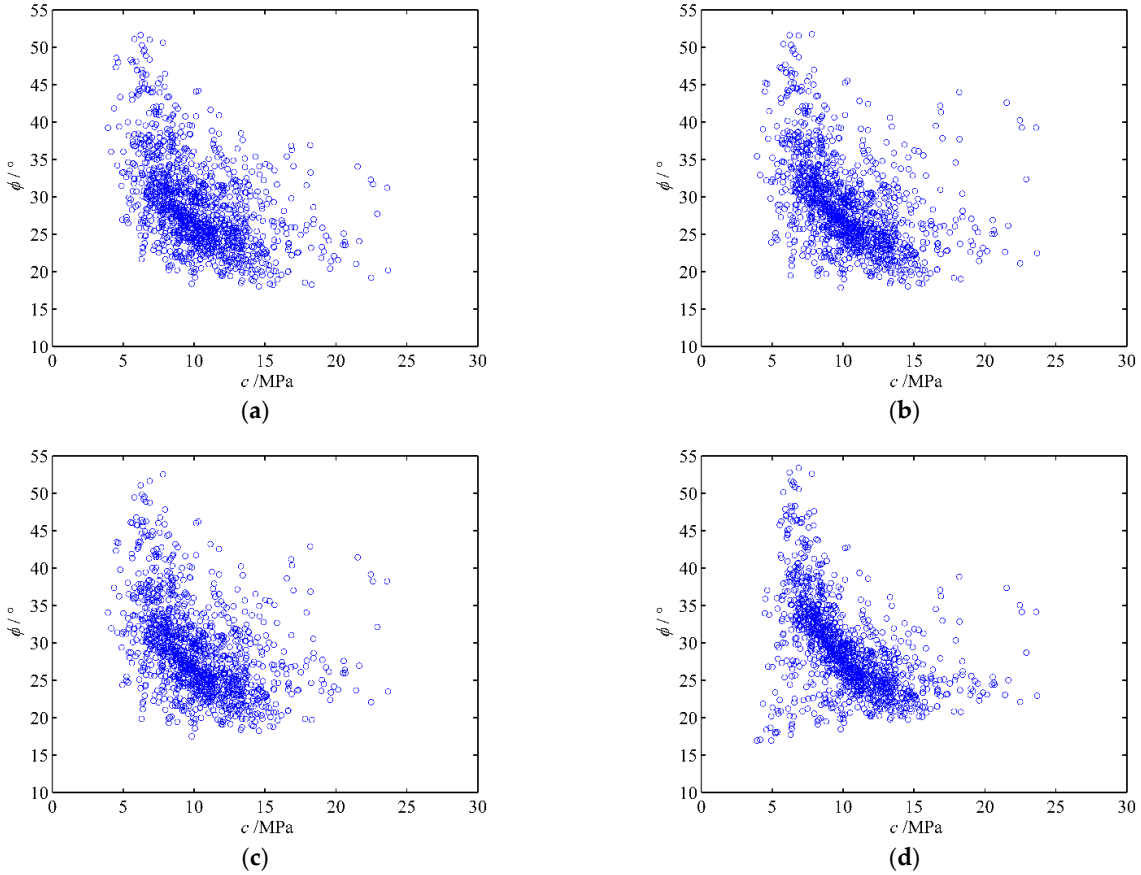

(**a**) (**b**) (**c**) (**d**)

Figure 8. Scatter plots of soil parameters associated with different CCRFs. (**a**) Gaussian copula. (**b**) Plackett copula. (**c**) Frank copula. (**d**) No. 16 copula.

To further verify the differences of the algorithms, Table 4 compares the average statistics of CCRFs via 1000 runs of algorithms. It can be observed that the cross-correlation coefficients of simulated c' and ϕ' associated with four candidate copulas are -0.5031, -0.4932, -0.4462 and -0.4879, which are almost similar to the original value of -0.5. Other statistics, including μ, σ, and COV, are also consistent with the original values. Namely, the proposed method recreates soil profiles similar to observations. This implies that the proposed copula-based CCRF is capable of considering the randomness, cross-correlation and spatial variability of soil parameters simultaneously, and effectively reflecting the real state of soil profiles with a relatively high accuracy.

Table 4. Statistics of CCRF variables associated with candidate copulas.

Copulas	ρ	τ	μ_c	σ_c	$\mathbf{COV}_c$	μ_ϕ	σ_ϕ	$\mathbf{COV}_\phi$
Gaussian	−0.5031	−0.3519	10.0787	3.0053	0.2982	29.9707	5.9839	0.1997
Plackett	−0.4932	−0.3739	10.0787	3.0053	0.2982	29.9686	5.9893	0.1999
Frank	−0.4462	−0.3326	10.0787	3.0053	0.2982	29.9658	5.9739	0.1994
No.16	−0.4879	−0.4133	10.0787	3.0053	0.2982	29.8598	6.0121	0.2011

For comparison, Figure 9 shows a typical realization of random fields without considering the cross-correlation of soil parameters. It can be seen that a homogeneous slope including two separate random field models is generated. Unlike Figures 6 and 7, c and ϕ are located in the meshes irregularly and independently. This can be explicated by corresponding scatter plots. In Figure 9c, the interdependency between c and ϕ is hardly clear. The scatters appearing in slope domains entirely rely upon the margins of c and ϕ, indicating that independent random fields are unable to describe the spatial cross-correlation of soil parameters. Such deficiency may result in inevitable uncertainty in the realization of spatially variable soil and subsequent geotechnical structure analysis. In contrast, the copula-based CCRF might be a preferable solution for realizing desirable random fields.

6.1.3. Effect of Marginal Distribution on CCRF

In this section, different margins are employed to model PDFs of c and ϕ. Comparisons among CCRFs associated with different margins are performed. A similar Gaussian copula is adopted as a control. Lastly, the effect of marginal distribution on CCRF is discussed.

Figures 10–12 respectively display the typical realizations of CCRFs associated with different candidate margins, namely, TN, TG and WB margins. The LN case is linked to Figure 4. For comparison, cases in which c and ϕ respectively hold TN and LN margins are also considered, as shown in Figure 13. Similar to Section 6.2, spatially variable soil can be efficiently demonstrated by the proposed method. c and ϕ develop smoothly in the horizontal direction and fluctuate severely in the vertical direction, reflecting their SOFs. In addition, it can also be clearly observed that a negative cross-correlation emerges between the two random fields. These observations are also successfully reproduced. It can also be seen that the margins of c and ϕ play important roles in modeling their spatial distributions. The ranges of c and ϕ with respect to different margins differ from each other. Comparably, the TG margins in Figure 11 generate the largest ranges of c and ϕ. However, the ranges yielded by TN margins in Figure 10 are almost similar to those induced by WB margins in Figure 12. Such differences would lead to different simulation results and further affect the final analysis of slope reliability.

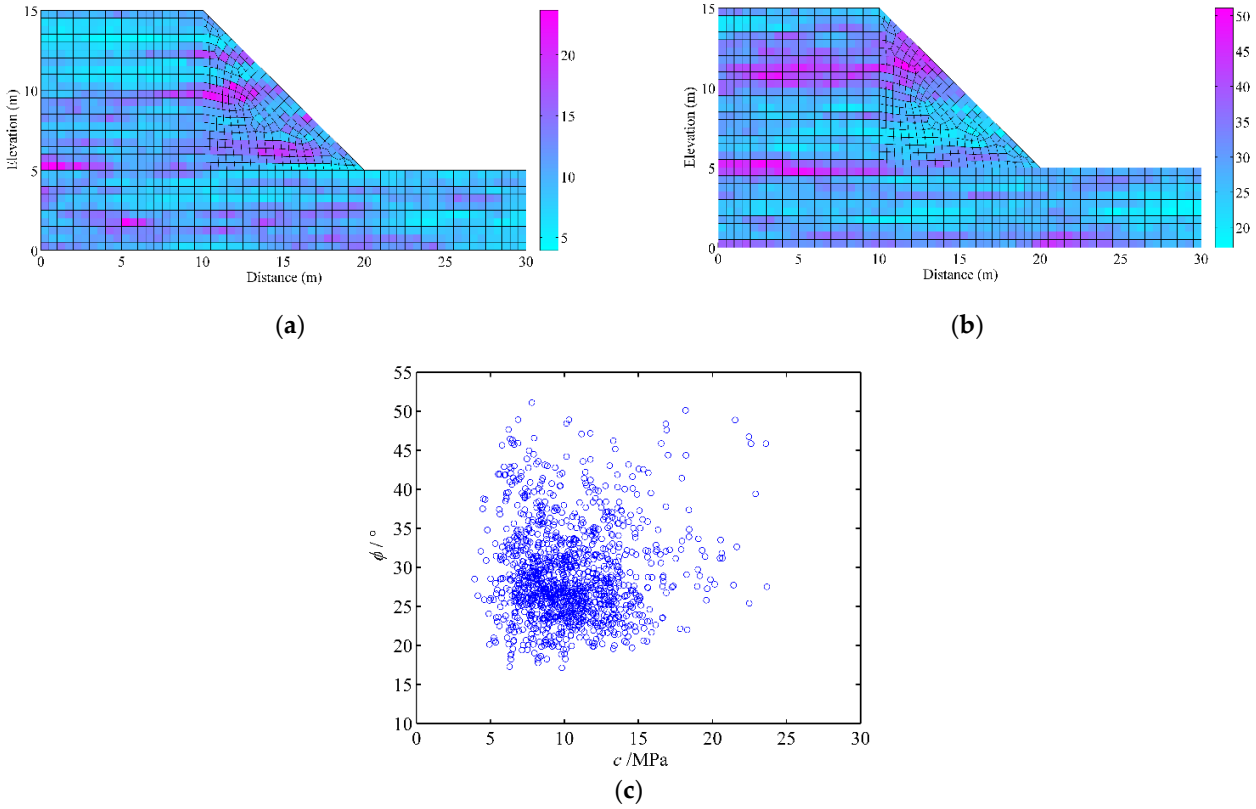

Figure 9. A typical realization of independent and non-correlation random field. (**a**) Random field of c. (**b**) Random field of ϕ. (**c**) Scatter plot of independent and non-correlation random field.

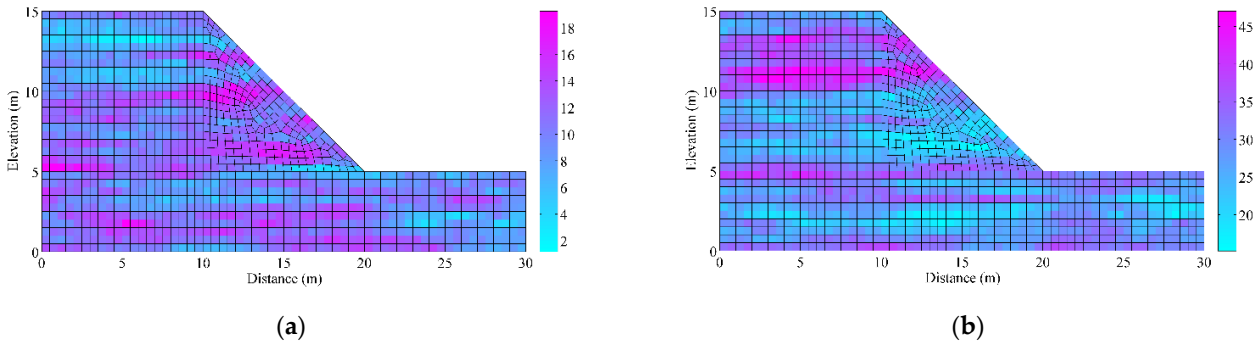

Figure 10. A typical realization of CCRF associated with TN margins. (**a**) Random field of c. (**b**) Random field of ϕ.

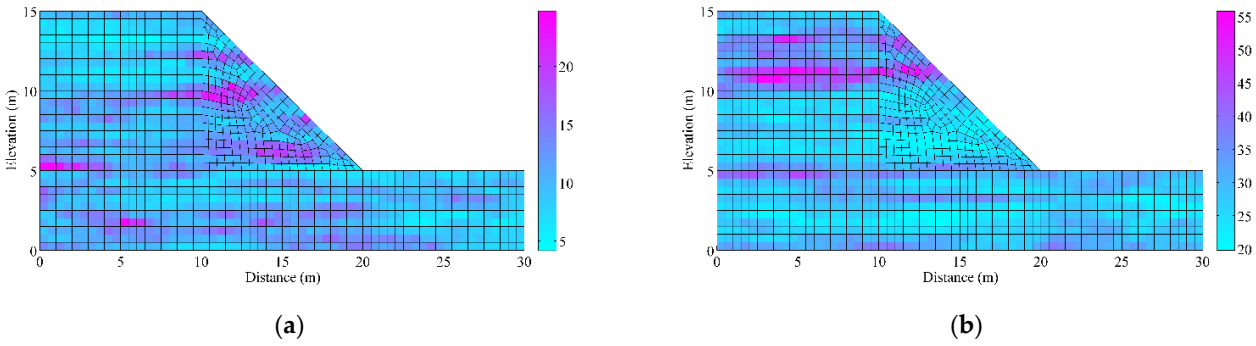

Figure 11. A typical realization of CCRF associated with TG margins. (**a**) Random field of c. (**b**) Random field of ϕ.

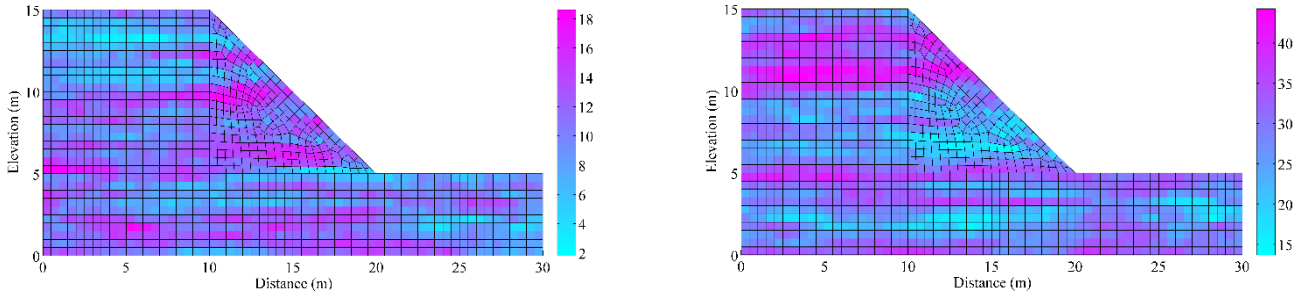

(**a**) (**b**)

Figure 12. A typical realizations of CCRF associated with WB margins. (**a**) Random field of c. (**b**) Random field of ϕ.

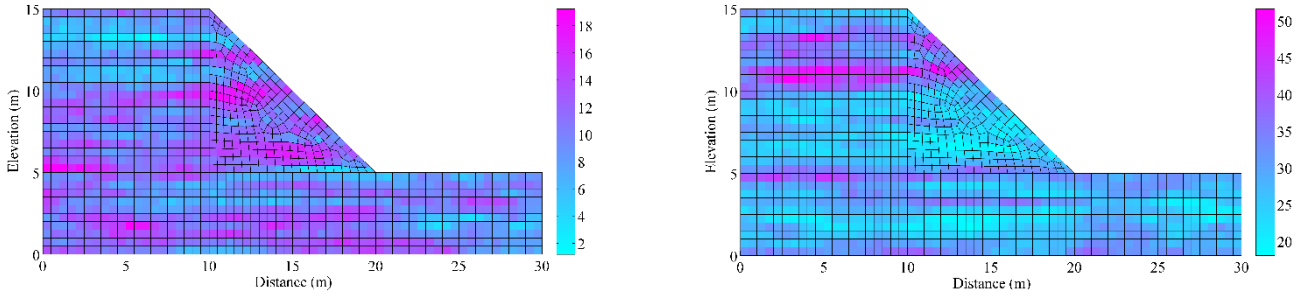

(**a**) (**b**)

Figure 13. A typical realization of CCRF associated with LN and TN margins. (**a**) Random field of c. (**b**) Random field of ϕ.

Figure 14 gives the scatter plots of four CCRFs. The LN case can be linked to Figure 8a. As expected, all five candidate cases yield negative dependence structures, which are consistent with the presented correlation direction. However, both the realizations of CCRF and the scatter plots of soil parameters associated with different margins are comparably inconsistent. This indicates that different margins correspond to different CCRF models. This is mainly due to the fact that the variables of RF obeying a uniform distribution in rank space are first yielded according to the Gaussian copula, and then transformed into the original space through the corresponding margins. Different margins would inevitably trigger differences in the generation of RFs. Therefore, the performance of copula-based CCRF is simultaneously governed by margins and copulas.

To further verify the proposed method, Table 5 compares the statistics of 2000 random variables generated by different margins. It can be inferred from Tables 4 and 5 that the cross-correlation coefficients of simulated c' and ϕ' associated with five cases are -0.5238, -0.4468, -0.5266, -0.5181 and -0.5031, which are very close to the original value of -0.5. Other statistical characteristics are also consistent with the original values. Namely, all five cases can recreate soil profiles similar to the observations. However, uncertain margins might lead to a slight bias in the simulation of spatially variable soil. Before implementing the proposed method, the margins of random variables should firstly be properly determined.

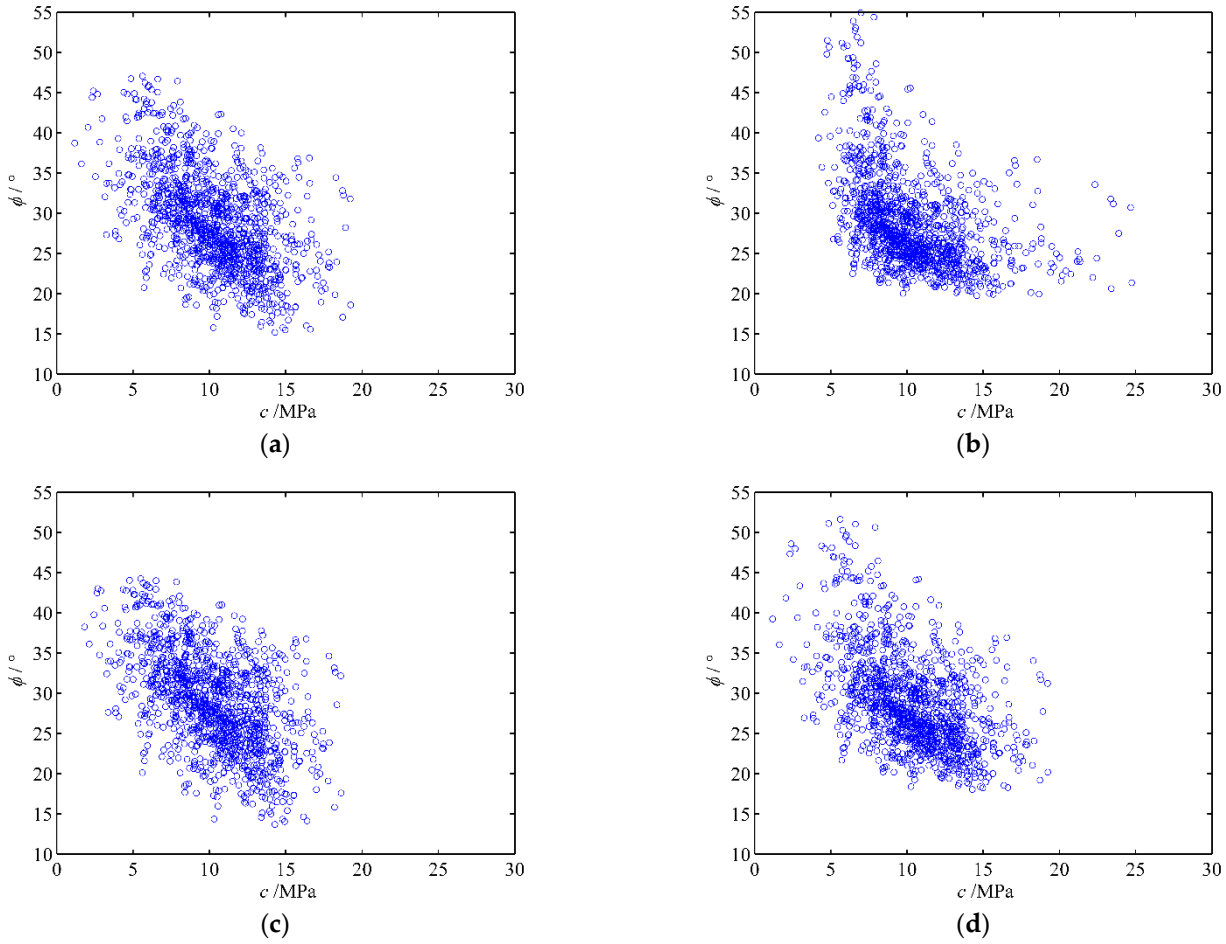

Figure 14. Scatter plots of soil parameters associated with different CCRFs. (**a**) TN margins. (**b**) TG margins. (**c**) WB margins. (**d**) LN and TN margins.

Table 5. Statistics of CCRF variables associated with candidate margins.

Margins	ρ	τ	μ_c	σ_c	COV_c	μ_ϕ	σ_ϕ	COV_ϕ
TN	−0.5238	−0.3682	10.297	2.995	0.2909	28.918	6	0.2075
TG	−0.4468	−0.3682	10.293	3.132	0.3043	29.038	6.036	0.2079
WB	−0.5266	−0.3682	10.29	2.999	0.2915	28.893	6.003	0.2078
LN and TN	−0.5181	−0.3682	10.297	2.995	0.2909	28.963	6.024	0.2080

6.1.4. Effect of Correlation Coefficient on CCRF

In order to further reveal the effect of cross-correlation on the CCRF, Figure 15 gives the variations of θ and $\rho_{c',\phi'}$ associated with different candidate copulas when the $\rho_{c,\phi}$ is changed between $[-0.9, -0.1]$. It is apparent that as $\rho_{c,\phi}$ increases, all four copula parameters θ increase accordingly. There is an obvious positive correlation between them. In addition, the $\rho_{c',\phi'}$ values of random variables recreated by different copulas are basically consistent with $\rho_{c,\phi}$, indicating the accuracy of the copula-based CCRF method. It is noticeable that there are slight differences among values of $\rho_{c',\phi'}$ corresponding to different copulas. This is mainly attributed to the fact that the joint distribution constructed by different copulas is different, although the same marginal distribution and correlation coefficient is employed. These results highlight the limitations in constructing cross-correlation random fields with cross-correlation coefficients. It is impossible to derive a unique cross-correlation structure with cross-correlation coefficients.

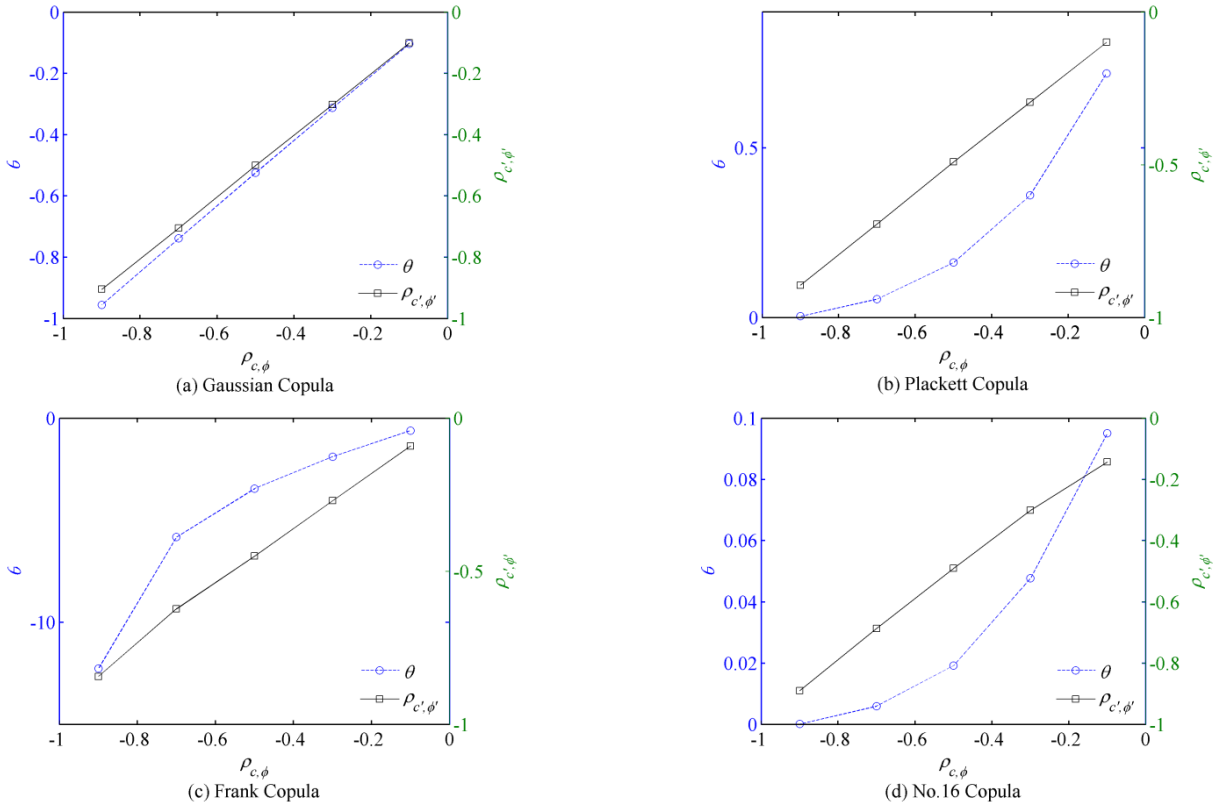

Figure 15. Copula parameters change with the correlation coefficient.

6.2. Example 2: Chicago Congress Street Cut Slope

6.2.1. The Profile of Chicago Congress Street Cut Slope

The geometry of the Chicago Congress Street cut slope [38] is shown in Figure 16. The height of the slope is 14.3 m. The slope comprises four layers, i.e., backfill sand in the first layer and three undrained clay layers beneath. The thickness of each layer is demonstrated in Figure 16. The statistics of soil parameters in each layer are shown in Table 6, in the which c and ϕ of the three clay layers are assumed to be random variables subjected to LN margins. The cross-correlation coefficient $\rho_{c,\phi}$ is assumed to be -0.5.

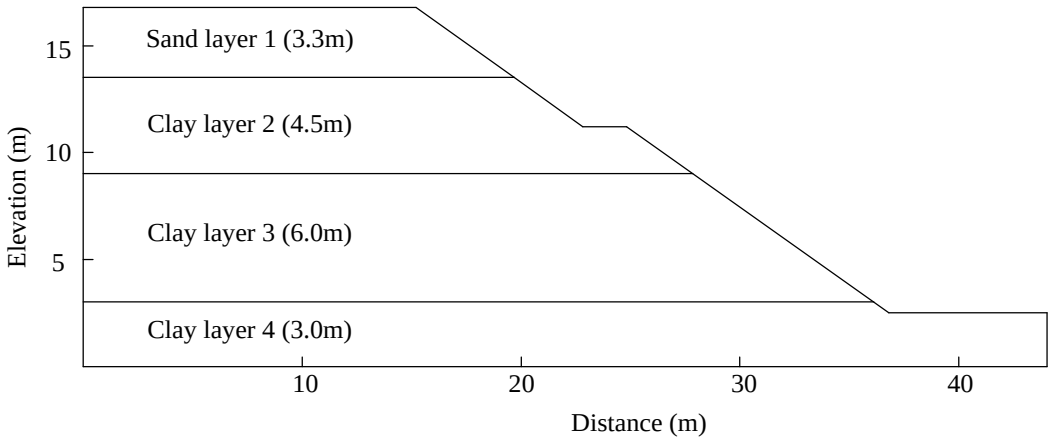

Figure 16. Chicago Congress Street cut slope.

Table 6. Statistics of soil parameters of the Chicago Congress Street cut slope.

Soil Layer	γ (kN/m^3)	c (kPa)			ϕ (°)		
		Margin	μ_c	COV$_c$	Margin	μ_ϕ	COV$_\phi$
Sand layer 1	21.0	-	0	-	-		-
Clay layer 2	19.5	LN	55	0.37	LN	5	0.2
Clay layer 3	19.5	LN	43	0.19	LN	7	0.21
Clay layer 4	20.0	LN	56	0.20	LN	15	0.24

To model the spatial distributions of c and ϕ, seven simulation strategies of multi-layer CCRFs are designed, as shown in Table 7. As for strategies 1–4, similar LN distributions are adopted to model margins of c and ϕ, but different dependent structures, namely, copulas, are utilized to realize the CCRF for the three clay layers. Strategy 4 assumes the independent appearance of geotechnical parameters, that is, $\boldsymbol{C}(\cdot) = 1$. As for strategies 5–7, similar combinations of copulas are assumed for three spatially variable layers, whereas different PDF types are implemented to model the margins of c and ϕ. With the aid of Algorithms 1–5, seven strategies are carried out, and the effects of uncertain copulas and margins on the generated multi-layer CCRFs are analyzed.

Table 7. Simulation strategies of multi-layer CCRFs.

Strategies	Margins	Copulas
Strategy 1	(LN, LN)	(Gaussian, Frank, Plackett)
Strategy 2	(LN, LN)	(Frank, Gaussian, No. 16)
Strategy 3	(LN, LN)	(Independent, Plackett, No. 16)
Strategy 4	(LN, LN)	(Independent, Independent, Independent)
Strategy 5	(TN, TN)	(Gaussian, Frank, Plackett)
Strategy 6	(TG, TG)	(Gaussian, Frank, Plackett)
Strategy 7	(WB, WB)	(Gaussian, Frank, Plackett)

6.2.2. Simulation of Multi-Layer CCRF

According to Table 7, seven typical realizations of multi-layer CCRFs associated with different simulation strategies are derived, as shown in Figures 17–23. It should be pointed out that all realizations are carried out based on the same seeds in rank space. It is obvious that, except for strategy 4, the rest successfully generate multi-layer CCRFs with the aid of copulas. Negative correlations can be clearly observed from their element colors, illustrating the feasibility of the proposed method in modeling spatially variable multi-layer soils. Moreover, strategies 1–4 yield the same RFs of c, which is due to the presence of the same seeds in each realization in rank space. However, the corresponding RFs of ϕ are considerably different from each other. Similar to the one-layer slope in Section 6, this is attributed to the fact that different copulas characterize different dependent structures, and therefore reproduce different CCRFs. From Figures 17 and 21, Figures 22 and 23, it can be seen that uncertain margins also affect the simulation of multi-layer CCRFs. Under similar dependent structures of geotechnical parameters, CCRFs transformed from standard space by different marginal PDFs show some differences. Therefore, before the probabilistic assessment of the slope system, deriving sufficient on-site observations of strata parameters is essential.

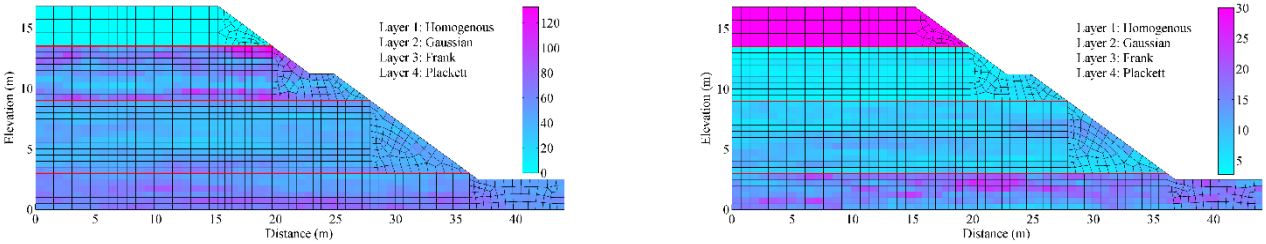

(**a**) (**b**)

Figure 17. A typical realization of transversely anisotropic CCRF yielded by strategy 1. (**a**) Random field of c. (**b**) Random field of ϕ.

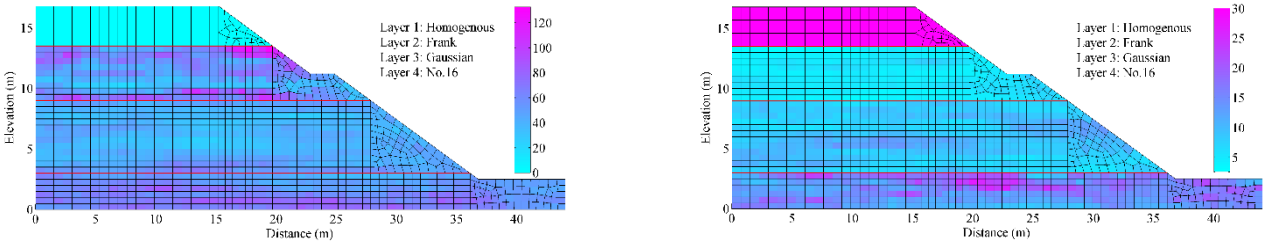

(**a**) (**b**)

Figure 18. A typical realization of transversely anisotropic CCRF yielded by strategy 2. (**a**) Random field of c. (**b**) Random field of ϕ.

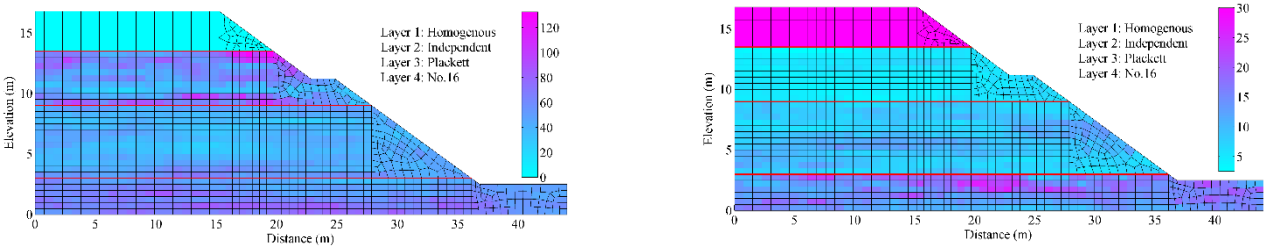

(**a**) (**b**)

Figure 19. A typical realization of transversely anisotropic CCRF yielded by strategy 3. (**a**) Random field of c. (**b**) Random field of ϕ.

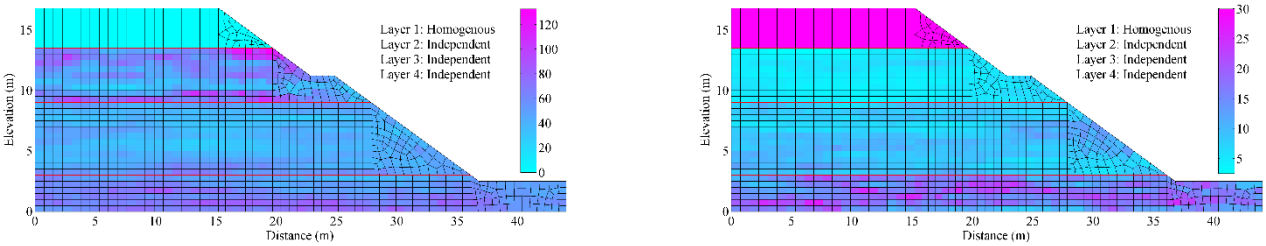

(**a**) (**b**)

Figure 20. A typical realization of transversely anisotropic CCRF yielded by strategy 4. (**a**) Random field of c. (**b**) Random field of ϕ.

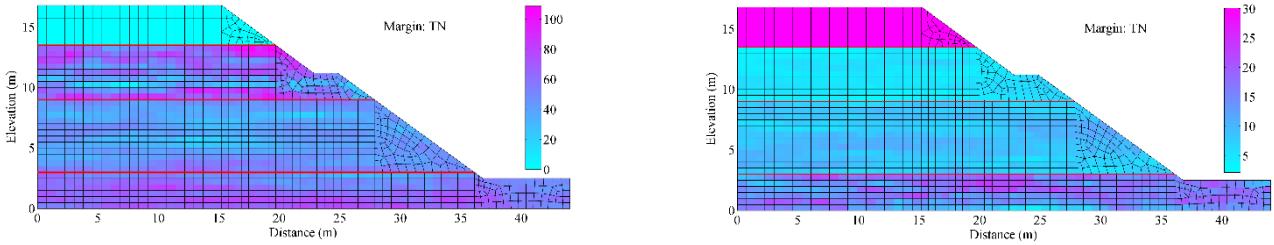

(**a**) (**b**)

Figure 21. A typical realization of transversely anisotropic CCRF yielded by strategy 5. (**a**) Random field of c. (**b**) Random field of ϕ.

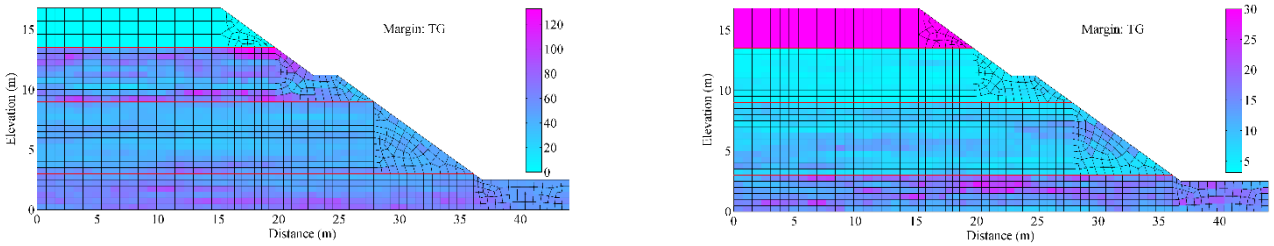

(**a**) (**b**)

Figure 22. A typical realization of transversely anisotropic CCRF yielded by strategy 6. (**a**) Random field of c. (**b**) Random field of ϕ.

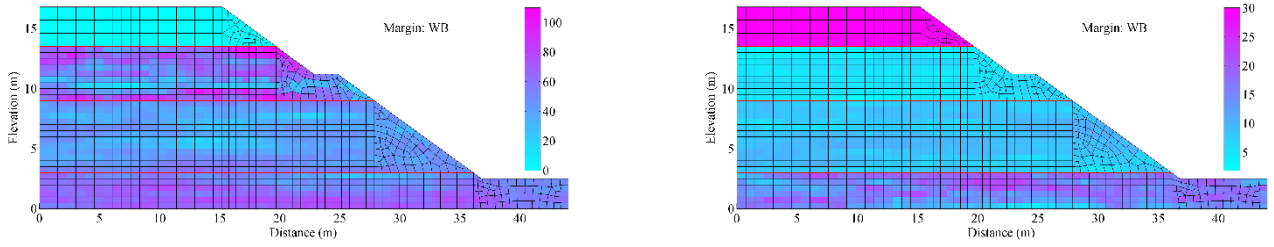

(**a**) (**b**)

Figure 23. A typical realization of transversely anisotropic CCRF yielded by strategy 7. (**a**) Random field of c. (**b**) Random field of ϕ.

Table 8 gives the statistics of multi-layer CCRFs associated with seven strategies. The corresponding average errors of the statistics with respect to three clay layers are shown in Figure 24. It can be seen that the average comprehensive errors of the seven cases are 4.62%, 4.96%, 10.72%, 23.87%, 6.47%, 5.96% and 7.14%, respectively. The statistics deduced by copula-based CCRF are basically consistent with the real values shown in Table 6. This demonstrates the accuracy of the proposed method in modeling multi-layer CCRFs for spatially variable soils. Notably, strategies 3 and 4 show a relatively high bias. This can be explained by the huge errors in the estimated $\rho_{c,\phi}$ values, as shown in Figure 24. In Strategy 3, the soil parameters of clay layer 1 are assumed to be independent variables, and yield 37.48% bias. This value under strategy 4 reaches 98.45% due to the neglect of dependent structures in all three clay layers. It can be concluded that ignoring the interdependency of soil parameters in the arbitrary layer of the slope would lead to significant deviation. Such bias would rapidly expand, as more faulty operations take place.

Table 8. Statistics of CCRF variables associated with different strategies.

Copulas	Soil Layers	μ_c	COV_c	μ_ϕ	COV_ϕ	ρ
Strategy 1	Layer 2	57.8521	0.3629	4.8705	0.2021	−0.5091
	Layer 3	41.5108	0.1901	8.6453	0.2109	−0.4383
	Layer 4	59.4741	0.1931	15.3436	0.2321	−0.5080
Strategy 2	Layer 2	57.8521	0.3629	4.8747	0.2073	−0.4639
	Layer 3	41.5108	0.1901	8.6081	0.2112	−0.5181
	Layer 4	59.4741	0.1931	15.0663	0.2375	−0.5602
Strategy 3	Layer 2	57.8521	0.3629	4.9316	0.1971	−0.0244
	Layer 3	41.5108	0.1901	8.6091	0.2115	−0.4735
	Layer 4	59.4741	0.1931	15.0663	0.2375	−0.5602
Strategy 4	Layer 2	57.8521	0.3629	4.9316	0.1971	−0.0244
	Layer 3	41.5108	0.1901	8.7082	0.2040	−0.0098
	Layer 4	59.4741	0.1931	16.1749	0.2279	0.0080
Strategy 5	Layer 2	58.0809	0.3468	4.8671	0.2055	−0.5254
	Layer 3	41.4723	0.1970	8.4923	0.1738	−0.4457
	Layer 4	59.4304	0.1885	15.3504	0.2365	−0.5116
Strategy 6	Layer 2	57.8589	0.3628	4.8763	0.1994	−0.4954
	Layer 3	41.5646	0.1848	8.7449	0.2400	−0.4179
	Layer 4	59.4177	0.1955	15.3251	0.2299	−0.4889
Strategy 7	Layer 2	57.9215	0.3550	4.8668	0.2071	−0.5243
	Layer 3	41.4660	0.2018	8.3971	0.1535	−0.4396
	Layer 4	59.3558	0.1849	15.3588	0.2365	−0.5031

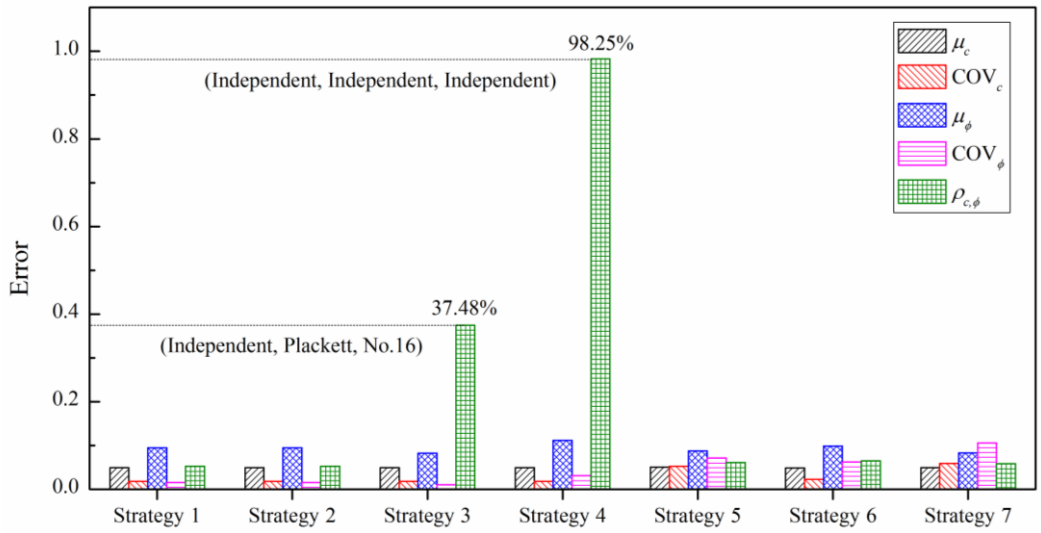

Figure 24. Average errors of the statistics with respect to the three clay layers deduced by different strategies.

6.3. Example 3: Papillion River Basin Slope

6.3.1. Soil Profile

To validate the application of the proposed method, a set of on-site observations of soil parameters in the Papillion River Basin slope, the United States, is adopted [39]. Figure 25 shows the scatters and corresponding empirical distributions of in-situ data from the Papillion River Basin of Brassica. The statistics are shown in Table 9. The density is assumed as a constant of 17 kN/m^3. The effect of the water table is ignored here. To model the Papillion River Basin slope with spatially variable c and ϕ, the same simplified slope geometry as that in Section 6 is used here.

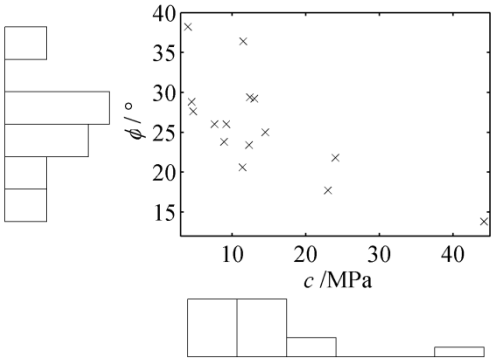

Figure 25. Observations of soil parameters in Papillion River Basin slope.

Table 9. Statistics of soil parameters in Papillion River Basin slope.

Soil Parameters	Statistics				
	μ	σ	COV	Pearson	Kendall
c	13.68	10.27	0.7511	−0.716	−0.4857
ϕ	25.85	6.36	0.2460		

6.3.2. Probability Distribution Estimation of Soil Parameters

To estimate the margins of soil profiles, goodness-of-fit tests, including *k-s* tests [40], AIC and BIC, are carried out to sieve out the optimal marginal types, as shown in Table 10. It can be seen that the LN distribution has the smallest D_n, AIC and BIC values. Therefore, the optimal margin distribution for modeling the c and ϕ of silty sand in the Papillion River Basin is LN.

Table 10. Goodness-of-fit test results of different margins.

Margins	c			ϕ		
	D_n	AIC	BIC	D_n	AIC	BIC
TN	0.2682	112.58	114.00	0.1548	101.06	102.48
LN	0.1367	105.11	106.52	0.1237	101.71	103.12
TG	0.2164	108.03	109.45	0.1320	103.48	104.90
WB	0.1817	108.73	110.14	0.1688	101.44	102.85

Subsequently, copula parameters are derived from the correlation coefficients shown in Table 9. Different copulas are constructed to characterize the cross-correlation between c and ϕ. The corresponding results of goodness-of-fit test are shown in Table 11. It can be seen that the Gaussian copula exhibits the smallest AIC and BIC scores, indicating that the Gaussian copula should be employed to characterize the cross-correlation between the c and ϕ values of silty sand in the Papillion River Basin slope.

Table 11. AIC and BIC scores of different copulas.

Copulas	Gaussian	Plackett	Frank	No. 16
AIC	−6.2223	−2.9015	−3.3795	3.2895
BIC	−5.5143	−2.1934	−2.6714	3.9976

6.3.3. Simulation of CCRF for Soil Parameters

In this section, a transversely anisotropic CCRF of the studied slope is constructed. It can be concluded from the previous section that the optimal margins of c and ϕ adopt the LN distribution. The optimal model representing the dependent structure of c and ϕ is the Gaussian copula. According to Algorithm 1 applied to the Gaussian-based CCRF proposed

in Section 4, a transversely anisotropic CCRF can be generated. A typical realization of this is shown in Figure 26. As expected, the spatial variability and cross-correlation of soil parameters can be successfully reproduced. The RF variables are distributed similarly to the measured data and can cover them well, demonstrating the efficiency of the proposed method.

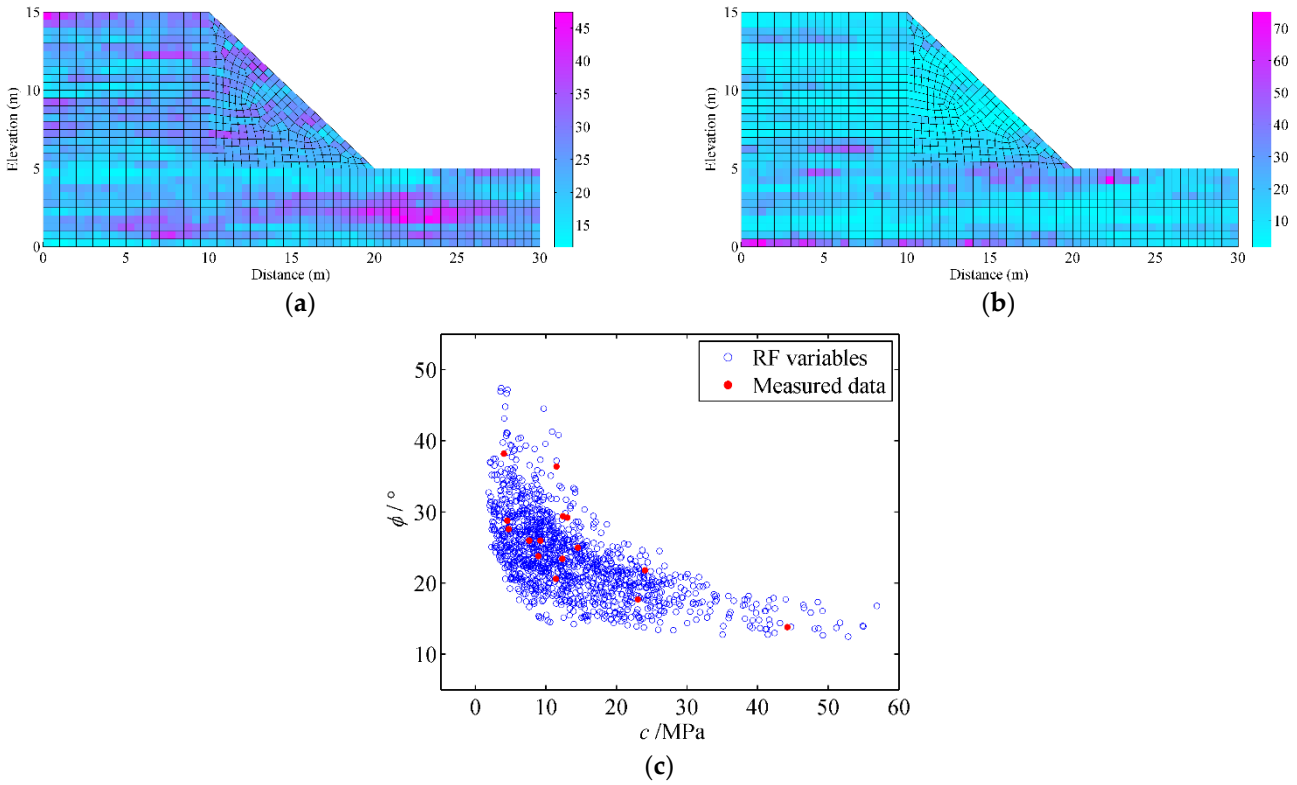

Figure 26. A typical realization of CCRF for soil parameters of the Papillion River Basin slope. (**a**) Random field of c. (**b**) Random field of ϕ. (**c**) Scatter plot of CCRF variables and measured data.

Table 12 gives the statistics of CCRF variables associated with candidate margins and copulas. The average comprehensive errors of the seven cases in Table 1 are 5.42%, 6.93%, 6.69%, 13.24%, 11.17%, 7.72% and 5.53%, respectively. The statistical characteristics of soil parameters are basically consistent. The proposed copula-based CCRF approach can better reflect the true distribution of cross-correlated soil profiles with a relatively high accuracy. Obviously, Gaussian copula-based CCRF in conjunction with LN margins can reflect the spatial distribution of soil parameters in the Papillion River Basin slope.

Table 12. Statistics of CCRF variables associated with candidate margins and copulas.

Margins	Copula	μ_c	COV_c	μ_ϕ	COV_ϕ	$\rho_{c,\phi}$	$\tau_{c,\phi}$
(LN, LN)	Gaussian	14.1232	0.7055	23.6476	0.2466	−0.6255	−0.4945
(LN, LN)	Plackett	14.1232	0.7055	23.4610	0.2513	−0.5815	−0.4755
(LN, LN)	Frank	14.1232	0.7055	23.5756	0.2527	−0.5777	−0.4855
(LN, LN)	No.16	14.1232	0.7055	23.4873	0.2622	−0.4617	−0.3938
(TN, TN)	Gaussian	16.0378	0.5499	23.5136	0.2704	−0.7000	−0.4945
(TG, TG)	Gaussian	14.9426	0.6617	23.7249	0.2364	−0.6355	−0.4945
(WB, WB)	Gaussian	14.2407	0.7232	23.4831	0.2770	−0.7033	−0.4945

7. Conclusions

Aiming at simulating the spatial variability of cross-correlated soil parameters, this paper proposes a method of simulating cross-correlated random fields for transversely

anisotropic soil slopes based on copulas. Four algorithms of CCRF obeying different dependent structures are established. The differences among CCRFs associated with different copulas are comparatively demonstrated. The effects of the cross-correlation and spatial variability of geotechnical parameters on the proposed copula-based CCRF are deeply discussed. Lastly, the feasibility and efficiency of the proposed method are verified by two examples. Some main conclusions can be drawn, as follows.

The distribution of random variables derived from independent random fields entirely depends on marginal distribution, which cannot account for the interdependency of soil parameters. On this account, independent random fields cannot reflect the real distribution of soil profiles. Subsequent structural stability analysis is bound to cause large deviation and uncertainty.

The copula-based CCRF accounts for the autocorrelation and cross-correlation of soil profiles simultaneously. It can be interpolated within each element to represent spatially variability. With the aid of the proposed method, the statistical characteristics of soil parameters can be recreated to agree with the observations. Soil profiles can be reflected with a relatively high accuracy.

The cross-correlation coefficient and copula affect the characterization of the dependent structure of CCRFs. A unique dependent structure cannot be determined from the marginal distribution and cross-correlation coefficient of soil parameters. Ignoring the interdependency of soil parameters would lead to significant bias, which might further expand as more negligence occurs. Therefore, it is not reasonable to construct the CCRF only using cross-correlation coefficient, which is often the case in reality.

The performance of the copula-based CCRF is simultaneously governed by the dependent structures and marginal distributions of random variables. Different copulas correspond to different CCRF models and interdependencies. Uncertain margins of soil parameters also affect the realizations of random fields. Before implementing the algorithm, the copula and margins of soil parameters should be precisely determined.

In addition, the CCRFs constructed by different copulas are very different. More algorithms derived from other copulas should be established to cater to various complicated dependent structures. Meanwhile, the proposed method in this paper is non-intrusive. It can therefore be employed in conjunction with the random finite element method. On this basis, further advanced and efficient slope reliability methods should be investigated in the future to reduce the computational burden caused by more and more complex algorithms.

Author Contributions: Conceptualization, X.Z. and H.X.; Methodology, X.Z. and Y.S.; Resources, X.Z. and H.X.; Data curation, Y.S.; Writing—review & editing, X.Z., H.X. and Y.S.; Project administration, X.Z. and H.X.; Funding acquisition, X.Z. and H.X. All authors have read and agreed to the published version of the manuscript.

Funding: This research was funded by the National Natural Science Foundation of China (52108315, 52078195), the Natural Science Foundation of Hubei Province of China (2021CFB286), the Youth Science and Technology Research Program of Hubei Education Department (Q20211404), the Joint Funds of the National Nature Science Foundation of China (U22A20232), and the Research Fund for the Doctoral Program of Hubei University of Technology (BSQD2020052).

Institutional Review Board Statement: Not applicable.

Informed Consent Statement: Not applicable.

Data Availability Statement: Some or all of the data, models, or code that support the findings of this study are available from the corresponding author upon reasonable request. The authors declare that they have no known competing financial interests or personal relationships that could have appeared to influence the work reported in this paper.

Conflicts of Interest: The authors declare that they have no known competing financial interest or personal relationships that could have appeared to influence the work reported in this paper.

References

1. Ali, A.; Huang, J.; Lyamin, A.V.; Sloan, S.W.; Griffiths, D.V.; Cassidy, M.J.; Li, J.H. Simplified quantitative risk assessment of rainfall-induced landslides modelled by infinite slopes. *Eng. Geol.* **2014**, *179*, 102–116. [CrossRef]
2. Jiang, S.H.; Papaioannou, I.; Straub, D. Bayesian updating of slope reliability in spatially variable soils with in-situ measurements. *Eng. Geol.* **2018**, *239*, 310–320. [CrossRef]
3. Liu, L.; Zhang, S.; Cheng, Y.M.; Liang, L. Advanced reliability analysis of slopes in spatially variable soils using multivariate adaptive regression splines. *Geosci. Front.* **2019**, *10*, 671–682. [CrossRef]
4. Tang, X.S.; Wang, M.X.; Li, D.Q. Modeling multivariate cross-correlated geotechnical random fields using vine copulas for slope reliability analysis. *Comput. Geotech.* **2020**, *127*, 103784. [CrossRef]
5. Wang, M.X.; Tang, X.S.; Li, D.Q.; Qi, X.H. Subset simulation for efficient slope reliability analysis involving copula-based cross-correlated random fields. *Comput. Geotech.* **2020**, *118*, 103326. [CrossRef]
6. Dasaka, S.M. Probabilistic Site Characterization and Reliability Analysis of Shallow Foundations and Slopes. Ph.D. Dissertation, Indian Institute of Science, Bengaluru, India, 2005.
7. Fenton, G.A.; Griffiths, D.V. Bearing-capacity prediction of spatially random c-ϕ soils. *Can. Geotech. J.* **2003**, *40*, 54–65. [CrossRef]
8. Zhou, X.; Zhang, G.; Hu, S.; Li, J. Optimal estimation of shear strength parameters based on copula theory coupling information diffusion technique. *Adv. Civ. Eng.* **2019**, *2019*, 873869. [CrossRef]
9. Zhou, X.; Zhang, G.; Hu, S.; Li, J.; Xuan, D.; Lv, C. Copula-based approach coupling information diffusion distribution for slope reliability analysis. *Bull. Eng. Geol. Environ.* **2020**, *79*, 2255–2270. [CrossRef]
10. Dasgupta, U.S.; Chauhan, V.B.; Dasaka, S.M. Influence of spatially random soil on lateral thrust and failure surface in earth retaining walls. *Georisk Assess. Manag. Risk Eng. Syst. Geohazards* **2017**, *11*, 247–256. [CrossRef]
11. Bayramoglu, I.; Gebizlioglu, O.L. A max–min model of random variables in bivariate random sequences. *J. Comput. Appl. Math.* **2021**, *388*, 113304. [CrossRef]
12. Cheng, H.; Chen, J.; Chen, R.; Chen, G. Comparison of Modeling Soil Parameters Using Random Variables and Random Fields in Reliability Analysis of Tunnel Face. *Int. J. Geomech.* **2019**, *19*, 04018184. [CrossRef]
13. Vanmarcke, E.H. Probabilistic modeling of soil profiles. *J. Geotech. Eng. Div.* **1977**, *103*, 1227–1246. [CrossRef]
14. Zhang, L.; Li, D.Q.; Tang, X.S.; Cao, Z.J.; Phoon, K.K. Bayesian model comparison and characterization of bivariate distribution for shear strength parameters of soil. *Comput. Geotech.* **2018**, *95*, 110–118. [CrossRef]
15. Tang, X.S.; Li, D.Q.; Zhou, C.B.; Phoon, K.K. Copula-based approaches for evaluating slope reliability under incomplete probability information. *Struct. Saf.* **2015**, *52*, 90–99. [CrossRef]
16. Do, D.M.; Gao, K.; Yang, W.; Li, C.Q. Hybrid uncertainty analysis of functionally graded plates via multiple-imprecise-random-field modelling of uncertain material properties. *Comput. Methods Appl. Mech. Eng.* **2020**, *368*, 113116. [CrossRef]
17. Yang, Z.; Li, X.; Qi, X. Efficient simulation of multivariate three-dimensional cross-correlated random fields conditioning on non-lattice measurement data. *Comput. Methods Appl. Mech. Eng.* **2022**, *388*, 114208. [CrossRef]
18. Dasaka, S.M.; Zhang, L.M. Spatial variability of in situ weathered soil. *Geotechnique* **2012**, *62*, 375–384. [CrossRef]
19. Napoli, M.L.; Barbero, M.; Ravera, E.; Scavia, C. A stochastic approach to slope stability analysis in bimrocks. *Int. J. Rock Mech. Min. Sci.* **2018**, *101*, 41–49. [CrossRef]
20. Pandit, B.; Tiwari, G.; Latha, G.M.; Babu, G.L.S. Probabilistic Characterization of Rock Mass from Limited Laboratory Tests and Field Data: Associated Reliability Analysis and Its Interpretation. *Rock Mech. Rock Eng.* **2019**, *52*, 2985–3001. [CrossRef]
21. Yang, R.; Huang, J.; Griffiths, D.V.; Sheng, D. Probabilistic stability analysis of slopes by conditional random fields. *Geo-Risk* **2017**, *2017*, 450–459. [CrossRef]
22. Liu, Y.; Zhang, W.; Zhang, L.; Zhu, Z.; Hu, J.; Wei, H. Probabilistic stability analyses of undrained slopes by 3D random fields and finite element methods. *Geosci. Front.* **2018**, *9*, 1657–1664. [CrossRef]
23. Jiang, S.H.; Huang, J.; Griffiths, D.V.; Deng, Z.P. Advances in reliability and risk analyses of slopes in spatially variable soils: A state-of-the-art review. *Comput. Geotech.* **2022**, *141*, 104498. [CrossRef]
24. Zhu, H.; Zhang, L.M.; Xiao, T.; Li, X.Y. Generation of multivariate cross-correlated geotechnical random fields. *Comput. Geotech.* **2017**, *86*, 95–107. [CrossRef]
25. Cho, S.E. Probabilistic Assessment of Slope Stability That Considers the Spatial Variability of Soil Properties. *J. Geotech. GeoEnviron. Eng.* **2009**, *136*, 975–984. [CrossRef]
26. Jiang, S.H.; Li, D.Q.; Zhang, L.M.; Zhou, C.B. Slope reliability analysis considering spatially variable shear strength parameters using a non-intrusive stochastic finite element method. *Eng. Geol.* **2014**, *168*, 120–128. [CrossRef]
27. Nelsen, R.B. *An Introduction to Copulas*; Springer: New York, NY, USA, 2006.
28. Nguyen, T.S.; Likitlersuang, S.; Tanapalungkorn, W.; Phan, T.N.; Keawsawasvong, S. Influence of copula approaches on reliability analysis of slope stability using random adaptive finite element limit analysis. *Int. J. Numer. Anal. Met.* **2022**, *12*, 46. [CrossRef]
29. Wu, X.Z. Trivariate analysis of soil ranking-correlated characteristics and its application to probabilistic stability assessments in geotechnical engineering problems. *Soils Found.* **2013**, *53*, 540–556. [CrossRef]
30. Wang, F.; Li, H. On the need for dependence characterization in random fields: Findings from cone penetration test (CPT) data. *Can. Geotech. J.* **2019**, *56*, 710–719. [CrossRef]

31. Masoudian, M.S.; Hashemi Afrapoli, M.A.; Tasalloti, A.; Marshall, A.M. A general framework for coupled hydro-mechanical modelling of rainfall-induced instability in unsaturated slopes with multivariate random fields. *Comput. Geotech.* **2019**, *115*, 103162. [CrossRef]
32. Griffiths, D.V.; Huang, J.; Fenton, G.A. Probabilistic infinite slope analysis. *Comput. Geotech.* **2011**, *38*, 577–584. [CrossRef]
33. Savvas, D.; Papaioannou, I.; Stefanou, G. Bayesian identification and model comparison for random property fields derived from material microstructure. *Comput. Methods Appl. Mech. Eng.* **2020**, *365*, 113026. [CrossRef]
34. Zheng, Z.; Dai, H. Simulation of multi-dimensional random fields by Karhunen–Loève expansion. *Comput. Methods Appl. Mech. Eng.* **2017**, *324*, 221–247. [CrossRef]
35. Zhu, H. *Probabilistic Evaluation and Field Testing of the Stability and Erodibility of Vegetated Slopes*; The Hong Kong University of Science and Technology: Hongkong, China, 2014.
36. Akaike, H. A New Look at the Statistical Model Identification. *IEEE Trans. Automat. Contr.* **1974**, *19*, 716–723. [CrossRef]
37. Lan, W.; Wang, H.; Tsai, C.L. A Bayesian information criterion for portfolio selection. *Comput. Stat. Data Anal.* **2012**, *56*, 88–99. [CrossRef]
38. Jiang, S.H.; Huang, J.S. Efficient slope reliability analysis at low-probability levels in spatially variable soils. *Comput. Geotech.* **2016**, *75*, 18–27. [CrossRef]
39. Soenksen, P.J.; Turner, M.J.; Dietsch, B.J.; Simon, A. *Stream Bank Stability in Eastern Nebraska*; USGS Rep 03-4265; U.S. Geological Survey: Lincoln, NE, USA, 2003; p. 102.
40. Smirnov, N. Table for Estimating the Goodness of Fit of Empirical Distributions. *Ann. Math. Stat.* **2007**, *19*, 279–281. [CrossRef]